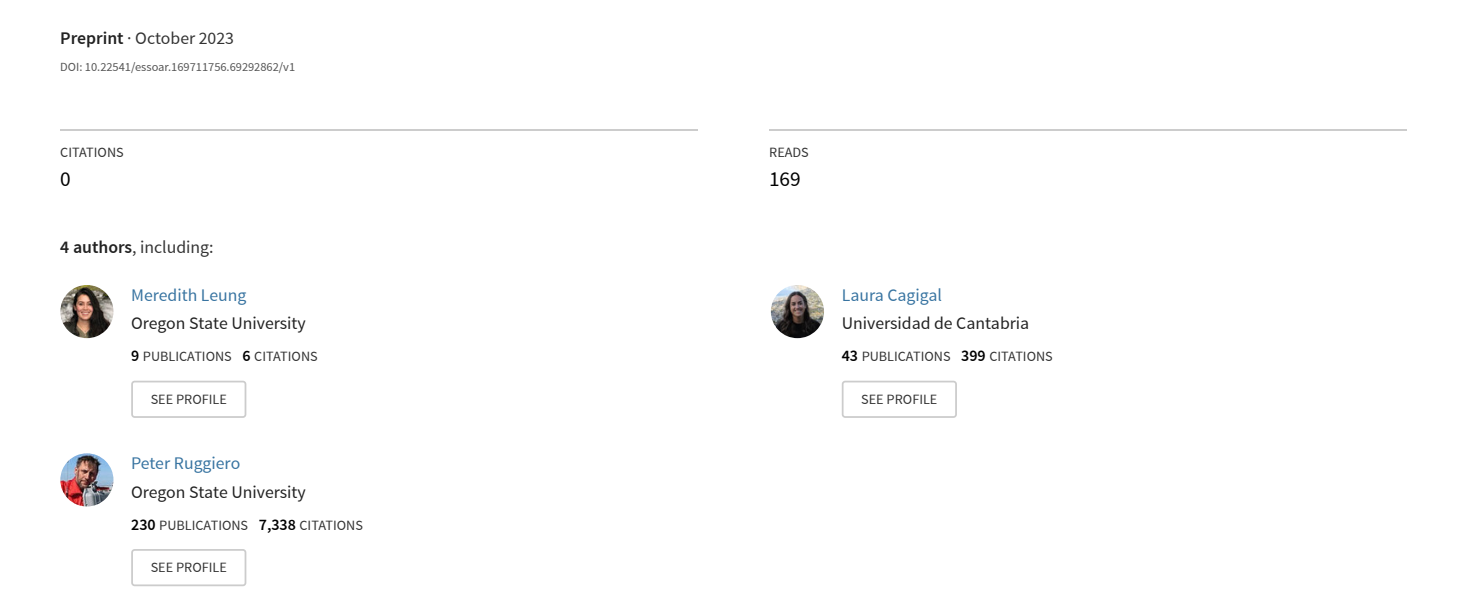
Projecting Future Chronic Coastal Hazard Impacts, Hotspots, and Uncertainty at Regional Scale



Projecting Future Chronic Coastal Hazard Impacts, Hotspots, and Uncertainty at Regional Scale

Meredith C Leung¹, Laura Cagigal², Fernando J. Méndez², and Peter Ruggiero¹

 1 Oregon State University

October 12, 2023

Abstract

While there is high certainty that chronic coastal hazards like flooding and erosion, are increasing due to climate change induced sea-level rise, there is high uncertainty surrounding the timing, intensity, and location of future hazard impacts. Assessments that quantify these aspects of future hazards are critical for adaptation planning under a changing climate and can reveal new insights into the drivers of coastal hazards. In particular, probabilistic simulations of future hazard impacts can improve these assessments by explicitly quantifying uncertainty and by better simulating dependence structures between the complex multivariate drivers of hazards. In this study, a regional-scale probabilistic assessment of climate change induced coastal hazards is conducted for the Cascadia region, USA during the 21st century. Three co-produced hazard proxies for beach safety, erosion, and flooding are quantified to identify areas of high hazard impacts and determine hazard uncertainty under three sea-level rise scenarios. A novel chronic coastal hazard hotspot indicator is introduced that identifies areas that may experience significant increases in hazard impacts compared to present day conditions. We find that Southern Cascadia and Northern Washington have larger hazard impacts and hazard uncertainty due to their morphologic setting. Erosional hazards, relative to beach safety and coastal flooding, will increase the most in Cascadia during the 21st century under all sea-level rise scenarios. Finally, we find that hazard uncertainty associated with wave and water level variability exceeds the uncertainty associated with sea-level-rise until the end of the century.

²Universidad de Cantabria

Projecting Future Chronic Coastal Hazard Impacts, Hotspots, and Uncertainty at Regional Scale

Meredith Leung¹, Laura Cagigal², Fernando Mendez², Peter Ruggiero¹

¹College of Earth, Ocean, and Atmospheric Sciences, Oregon State University, Corvallis, OR, USA

²Departamento Ciencias y Tecnicas del Agua y del Medio Ambiente, Universidad de Cantabria, Santander, Spain

Corresponding author: Meredith Leung (<u>leungmer@oregonstate.edu</u>)

Key Points:

- A regional assessment of 21st C coastal erosion, flooding, and unsafe beach hazard impacts and uncertainty is conducted for Cascadia, USA
- High hazard impacts and high rates of hazard change are focused in Northern and Southern Cascadia and are correlated with local morphology
- Hazard uncertainty driven by wave and water level variability is greater than uncertainty from sea level rise scenarios in the 21st C.

Abstract

While there is high certainty that chronic coastal hazards like flooding and erosion, are increasing due to climate change induced sea-level rise, there is high uncertainty surrounding the timing, intensity, and location of future hazard impacts. Assessments that quantify these aspects of future hazards are critical for adaptation planning under a changing climate and can reveal new insights into the drivers of coastal hazards. In particular, probabilistic simulations of future hazard impacts can improve these assessments by explicitly quantifying uncertainty and by better simulating dependence structures between the complex multivariate drivers of hazards. In this study, a regional-scale probabilistic assessment of climate change induced coastal hazards is conducted for the Cascadia region, USA during the 21st century. Three co-produced hazard proxies for beach safety, erosion, and flooding are quantified to identify areas of high hazard impacts and determine hazard uncertainty under three sea-level rise scenarios. A novel chronic coastal hazard hotspot indicator is introduced that identifies areas that may experience significant increases in hazard impacts compared to present day conditions. We find that Southern Cascadia and Northern Washington have larger hazard impacts and hazard uncertainty due to their morphologic setting. Erosional hazards, relative to beach safety and coastal flooding, will increase the most in Cascadia during the 21st century under all sea-level rise scenarios. Finally, we find that hazard uncertainty associated with wave and water level variability exceeds the uncertainty associated with sea-levelrise until the end of the century.

Plain Language Summary

We know that chronic coastal hazards such as erosion and flooding are growing more frequent and intense due to climate change, but it is difficult to determine exactly when, where, and how bad these hazards will be in the future. Constraining our predictions of the 'when, where, and how bad' is critical if we want to make management decisions that limit potential negative consequences for coastal communities. In this study, we partnered with stakeholders in the Cascadia Region, USA (northern California to northern Washington) to assess chronic coastal hazard impacts and hazard uncertainty. We use a probabilistic modeling approach to simulate flooding, erosion, and beach safety hazards from 2020-2100 under three sea-level-rise scenarios. We identify areas in Northern California, Southern Oregon, and Northern Washington, that will experience more hazardous conditions *and* a more rapid increase in hazards in the 21st century than elsewhere in the region. We find that erosion will increase more rapidly than unsafe beach and flooding hazards across Cascadia and all sea-level-rise scenarios. Lastly, we find that wave and water level variability is a greater contributor to hazard uncertainty than sea-level-rise throughout most of the 21st century and therefore should not be neglected in near-term adaptation planning.

1 Introduction

Chronic coastal hazards such as flooding and erosion are increasing in frequency and severity due to climate change induced sea-level rise (SLR) and changes in storminess patterns (e.g., Erikson et al., 2022; Moftakhari et al., 2015; Sweet et al., 2022). These hazards translate into extensive economic costs (e.g., inundation of infrastructure, loss of land and critical ecosystems; Chu-Agor et al., 2011; Martello & Whittle, 2023) and social costs (e.g., displacement, loss of community and community resources, limited mobility; Oppenheimer et al., 2019; Otto et al., 2017). However, much remains unknown about how climate change will influence the timing, intensity, and location of future chronic coastal hazards. Even more uncertain is the socioecological fallout of coastal squeeze, as the impacts of coastal hazards propagate inland through

different ecosystems (Mills et al., 2016). As such, hazard assessments at multiple spatial and temporal scales are needed to inform appropriate climate-aware adaptation strategies aimed at alleviating future costs of climate change induced coastal hazards (Toimil et al., 2023).

Regional scale hazard studies are particularly useful for guiding adaptation, as they align well with traditional governmental decision-making spatial scales and timelines (Barros et al., 2014; Hibbard et al., 2013). However, they remain extremely rare in coastal adaptation literature, comprising less than 3% of case studies (Cabana et al., 2023). Refining estimates of future uncertainty in hazard assessments is also a critical issue, for both fundamental coastal hazard science as well as for applied studies addressing impacts to communities (Hinkel et al., 2021; Splinter et al., 2021; Toimil et al., 2020). While more and more coastal change and coastal hazard studies are incorporating uncertainty analysis into their projections (e.g., Le Cozannet, et al., 2019; Vitousek et al., 2017), typically they only address the uncertainty associated with different carbon emission and sea-level rise scenarios (Vousdoukas et al., 2018). Neglecting other sources of uncertainty (e.g., variability in storminess patterns) can significantly truncate the projected range of outcomes, which, when passed on to coastal communities, can ultimately result in misinformed or maladaptive policy decisions (Boumis et al., 2023; Toimil et al., 2021).

Extreme value analysis (EVA) approaches are commonly adopted in impact assessments of future chronic coastal hazards (e.g., Taherkhani et al., 2020; Vousdoukas et al., 2020). These approaches use statistical techniques to characterize the frequency and intensity of previously unseen events based on the probability of hazardous extremes in the historical record. These techniques are powerful, generalizable, and well suited to practical applications (e.g., engineering design or insurance) because they quantify hazards in terms of traditional design criteria (e.g., extreme event return periods). EVA approaches can, however, be less suited to hazard analyses that explore both extreme and non-extreme conditions together or how the event timing influences impacts, as traditional EVA techniques typically explore the impacts of extremes in isolation (Wahl et al., 2017). Furthermore, EVA approaches can be challenged to accurately quantify extremes for hazards with complex multivariate drivers, as the dependence between drivers can be difficult to represent in these traditional frameworks (Hamdi et al., 2021).

Probabilistic simulation modeling (e.g., Callaghan et al., 2008, Serafin & Ruggiero, 2014) is an alternative approach to assessing future hazards that can avoid some of the typical drawbacks of EVA. Probabilistic methods can simulate a range of potential outcomes, representing both non-extreme and extreme conditions by varying the timing and intensity of the environmental variables that drive hazards. This approach enables exploration of how the timing of events can shape hazard impacts and can help dissect which environmental variables ultimately drive hazardous conditions (e.g., Serafin et al., 2017, Toimil et al., 2021). When combined with climate aware approaches that incorporate the uncertainty associated with forecasted carbon emission scenarios, regional sealevel rise (SLR) rates, decadal to intra-decadal oscillations in climate variability, etc., probabilistic approaches become a powerful tool for assessing and constraining the uncertainty of future hazard impacts (Kopp et al., 2019).

In this study, we employ a probabilistic approach to assess chronic coastal hazards in the 21st century at regional scale in Cascadia, USA. A stochastic climate emulator, developed and validated for several sites in the Pacific Basin (Anderson et al., 2019; Marra et al., 2022), is used to generate hourly time series of total water level (TWL) drivers for Cascadia open coast beaches from 2020-2100. We combine TWL drivers with three sea-level rise scenarios and propagate them onshore using wave transformation metamodels and empirical runup formulas to 100m resolution

along the coast. Using simple hazard proxies for beach safety, erosion, and flooding, we quantify the evolution of chronic coastal hazard impacts and uncertainty. This modeling approach produces high spatial and temporal resolution time series of potential hazard impacts in the Cascadia region and enables a climate-aware, probabilistic understanding of how hazards may evolve under climate change. We identify areas of high hazard impacts and determine which hazards dominate throughout the 21st century. We further locate hazard change hotspots, areas that currently see relatively little hazard activity, but will experience large increases in the future. This is an emerging priority for hazard planners, as these areas may be underprepared for hazardous conditions based on assumptions of safety informed by previous experience (Thompson et al., 2023). These areas are also important to identify as they are prime candidates for proactive climate-informed adaptation.

The paper is organized into 6 sections. In section 2, we describe the Cascadia coastline and provide background on chronic coastal hazards in the region. Section 3 details the methodology, models, and hazard proxy frameworks used in this study. In section 4, we describe the evolution of hazards under the three sea-level rise scenarios and their associated uncertainty, as well as the quantification and identification of hazard hotspots. Finally, sections 5 and 6 are comprised of discussion and conclusions.

2 Study Setting: The Cascadia Coastline

The outer US Cascadia coastline is approximately 950 km long, ranging from Northern California to the Straits of Juan de Fuca at the border between Washington state and Canada (Figure 1). Its longitudinal extent is defined by tectonic plate boundaries, namely the subduction of the Juan de Fuca and Gorda Plates under the North American Plate. Due to its tectonic setting, the Cascadia region faces an imminent nearfield rupture of the Cascadia Subduction Zone with a resultant earthquake (magnitude ranging from ~7.0-9.0) and tsunami (Atwater, 1987; OSSPAC, 2013). There is growing investment and motivation in the region to understand and prepare for a wide range of coastal hazards in Cascadia (earthquake, tsunami, and climate change). Stakeholders in the region have also emphasized the need for coastwide analyses that can integrate knowledge across different political and cultural boundaries (e.g., OSSPAC, 2013; Ruckelshaus Center, 2017). This analysis is aimed at better characterizing the impacts and uncertainty associated with chronic, climate change induced coastal hazards as part of this effort.

The tectonic setting of Cascadia also contributes to substantial vertical land motion (VLM) variability along the coast, translating to regional variability in relative sea-level rise rates (RSLR) (Figure 1). In some areas of Cascadia, VLM has been able to keep pace with increases in sea level (Burgette et al., 2009; Komar et al., 2011). However, in other areas of Cascadia the situation is more dire. For example, Humboldt Bay, CA is subsiding rapidly, resulting in local RSLR rates of approximately 6mm/yr (Anderson, 2018).

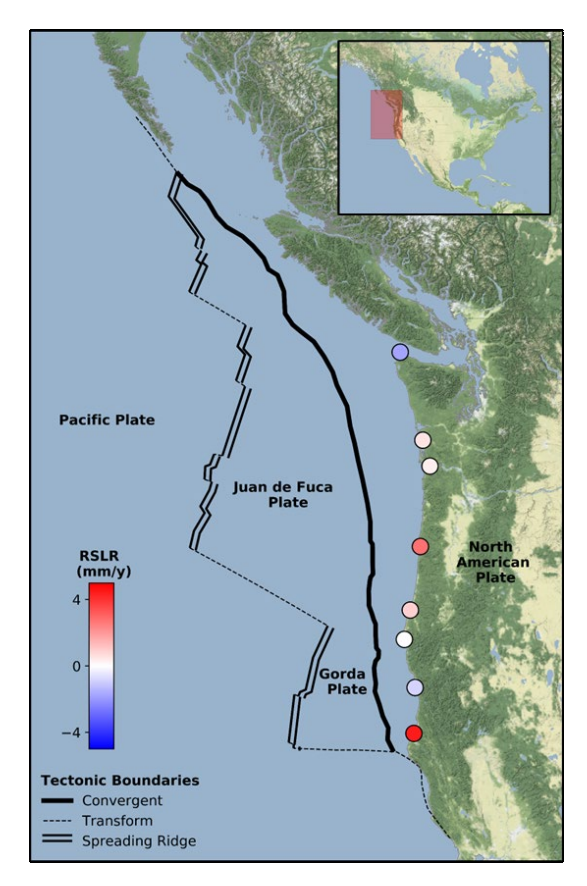


Figure 1. Cascadia Region with fault lines (Staisch and Walton, 2022) and historical regional sea level rise rates (NOAA Tides and Currents)

The Cascadia region experiences mixed semi-diurnal tides with a tidal range of 2-4 meters. The wave climate of the Cascadia region is also notable for its severity. Winter storms frequently produce long period waves with heights exceeding 9-10m (Komar et al., 2013; Tillotson & Komar, 1997), although there is some alongshore variability in wave conditions. While central and northern Cascadia experience mean wave heights up to 0.5 meter higher than southern Cascadia, the southern region tends to receive more long period (>20s) waves from the south (Smith et al., 2020). The Cascadia wave climate can be especially damaging to coastal infrastructure and road networks when compounded with elevated water levels (Serafin et al., 2017). El Nino Southern Oscillation (ENSO) events contribute to increased flood risk and hotspot erosion in the region due to more extreme winter waves (~30% higher) and higher water levels (~0.2-0.3m) than typical (Barnard et al., 2015; Barnard et al., 2017; Komar et al., 2011; Shope et al., 2022; Vos et al., 2023). While storm surges greater than 1.0 m have been observed in the region, surge typically contributes less than 0.3m to TWLs, due to the relatively narrow continental shelf and lack of tropical storms (Ardhuin et al., 2003; Serafin et al., 2017).

The outer coast of the Cascadia region is largely comprised of sandy beaches (58%), with some stretches of mixed sediment and cobble beaches (27% and 4% respectively). Approximately 34% of all beaches on the outer coast of the Cascadia region, regardless of sediment type, are cliff or bluff backed. Of the sandy beaches, 80% are backed by dunes while 4% are armored with riprap (Shope et al., 2022). Cliffs and bluffs in Cascadia tend to be comprised of consolidated layers of mud, sand, and gravel, and often are fronted by a thin veneer of eroded gravel (Ruggiero et al.,

2013). Dunes in the Cascadia region are highly vegetated with non-native grasses that produce tall, linear features and provide some protection from erosion and flooding hazards to the communities and ecosystems behind them (Ruggiero et al., 2018). However, while some communities in the Cascadia region are planting dune grasses to mitigate erosion and stabilize backshore systems, other communities bulldoze dunes to improve viewsheds and move sand away from infrastructure. Riprap is the most common solution employed to stem erosion hazards in Cascadia. However, increasingly, communities are attempting natural and nature-based solutions to provide more ecosystem services and contend with government restrictions protecting public beach access (Bond, 2021). Coastal management practices in the Cascadia region are further complicated by extensive protections for endangered species habitats, including the western snowy plover (Biel et al., 2017).

Many Cascadia coastal communities have already begun to experience increased coastal erosion rates and nuisance flooding events due to the combination of land management practices and climate change effects (e.g., Light, 2021; Anderson, 2018; Quinault Indian Nation, 2017). While individuals in Cascadia adapt to these changes on a parcel-by-parcel basis (e.g., by armoring property, Dundas & Lewis, 2020), there is debate among communities surrounding equitable adaptation and the role of the government in managing it (Lipiec et al., 2018; Mills et al., 2021). Developing a better understanding of future hazard exposure is therefore critically important to adopting adaptive measures, at both an individual and community scale.

3 Methods

We generated stochastic simulations of future TWLs from 2020-2100 for the Cascadia Region using the model framework TESLA (Time-varying Emulator for Short and Long-Term Analysis of coastal flooding and erosion; Anderson et al., 2019) in combination with three sealevel rise scenarios associated with 0.5m, 1.0m, 1.5m of global mean (GM)SLR by 2100 (Sweet et al., 2022) (fig. 2). The SLR scenarios of Sweet et al. (2022) are regionally corrected to probabilistically incorporate uncertainties associated with local processes (e.g., VLM and gravitational, rotational, and deformational changes caused by ice-mass loss). In this study we selected the median probability cases for each of the three SLR scenarios, focusing on producing TWLs that capture the range in probability associated with storminess and wave climate variability, which can produce differences in water level elevation on the order of decimeters to meters. TWLs represent the maximum elevation that water reaches on the coast. They are driven by atmospheric, oceanographic, and geomorphic processes and can be represented by the following equation (Serafin & Ruggiero, 2014):

$$TWL = \eta_{MSL} + \eta_{AT} + \eta_{SS} + \eta_{MMSL} + R_{2\%}$$
 (1)

where η_{MSL} is mean sea level, η_{AT} is the deterministic astronomical tide, η_{SS} describes the atmospheric driven storm surge, η_{MMSL} represents interannual variability captured through monthly mean sea level (MMSL), and $R_{2\%}$ represents the wave driven runup (2% exceedance level, e.g., Holman, 1986).

TWLs were simulated in two phases: first, through the simulation of offshore boundary conditions at eight semi-coupled TESLA nodes; and second, through nearshore transformation of wave conditions using wave transformation metamodels and empirical runup formulas (Figure 3). Onshore TWLs were used to conduct regional impact analyses at 100m resolution based on simple hazard proxies for unsafe beaches, erosion, and flooding derived from well-known coastal

frameworks and stakeholder engagement. Hazard indices were developed to determine joint hazard impacts and rates of hazard change.

An advisory council was consulted throughout project development through quarterly to semi-annual meetings. The council was directly involved in formulating research questions by identifying coastal community knowledge needs, co-producing the hazard proxies included in the study, and providing feedback on preliminary results. Advisory council members included federal and state agency employees, county commissioners, planners and emergency managers, city planners and city emergency managers, non-profit organizations, and academics. By design, this co-productive approach (Kates et al. 2000) produces new knowledge for the benefit of both the involved communities and researchers. Furthermore, it grows adaptive capacity through network building and the development of social capital (Norström et al., 2020).

3.1 Generating Probabilistic Future Total Water Levels

3.1.1 Statistical Simulation of Offshore Total Water Level Drivers

We used the stochastic climate emulator, TESLA (Anderson et al., 2019), to simulate 100 hypothetical chronologies of hourly TWL drivers from 2020-2100 based on statistical relationships derived from observations of present-day climate. This approach generates time series that represent the full range of water levels, as it captures the inherent randomness of individual processes that superimposed can compound or dampen the overall TWL signal. The TESLA methodology to create probabilistic simulations of hydrodynamic variables representing present day climate has been applied and validated at several sites globally (Anderson et al., 2021; Marra et al., 2020; d'Anna et al., 2022, Marra et al., 2022;; Vitousek et al., 2021). We provide a short summary of the methodology and Cascadia-specific validation below.

TESLA uses a weather type-based approach (Camus et al., 2014), in which annual weather types (AWTs), intra-seasonal weather types (IWTs), and daily weather types (DWTs) are defined based on observed atmospheric and oceanographic variables (fig. 2). Following the methodology presented in Anderson et al. (2019), we define six AWTs corresponding to conditions representative of El Niño, La Niña, and transition phases of ENSO. IWTs in turn represent changes in the Madden Julian Oscillation, and DWTs reflect synoptic weather patterns in the Pacific Basin. New chronologies of the weather types are generated via auto-logistic regression models that are able to reproduce the persistence, transition, and probability of occurrence of the weather types reflective of historical observations and model covariates (Antolinez et al., 2016).

The datasets used to define AWTs, IWTs, and DWTs make up the *predictors* in the TESLA framework. These datasets include sea surface temperature reanalysis products to classify AWTs (Extended Reconstructed Sea Surface Temperature v4, i.e., ERSSTv4; Huang et al., 2015), outgoing longwave radiation timeseries to cluster MJO intensity and location into IWTs (Wheeler & Hendon, 2004), and CFSR sea level pressure and sea level pressure gradient fields to create DWTs (Saha et al., 2011). The *predictands*, or the outputs of TESLA, include wave characteristics (wave height, period, and direction) and non-tidal residuals (MMSL and storm surge). Historical observations of the predictands are derived from wave hindcasts from the Center for Australian Weather and Climate Research (CAWCR; Durrant et al., 2014; Smith et al., 2020) and tide gauges (NOAA, tidesandcurrents.noaa.gov). Tide gauge water level data were corrected for vertical datum bias where necessary (Burgette et al., 2009) and decomposed into their constituent parts (η_{AT} , η_{SS} ,

 η_{MMSLA}) following the methodology presented in Serafin and Ruggiero (2014). The observed wave and water level datasets are used to populate statistical models (e.g., copulas and linear regression) that are used to connect the predictors and predictands.

The predictands are simulated to an hourly timescale for each synthetic WT timeseries through a multistep process. First, consecutive days of the same DWTs are grouped together as we assume they represent the same synoptic weather system or storm. Each weather event is assigned an event hydrograph that represents the ramp up to and ramp down from maximum potential wave height within that weather system and is designed to maintain physically realistic joint dependence of sea state parameters. Synthetic wave hydrographs are generated based on random sampling of parameterized historical hydrographs during the specified DWT sea state using gaussian copulas (Anderson et al., 2019). Employing gaussian copulas maintains the historical dependence structures between sea state parameters and weather types while allowing for extrapolation from historical observations (Cagigal et al., 2020). While wave height evolves hourly based on hydrograph ramp up and down, other variables (Tp, Dir, and η_{SS}) remain static for the duration of the hydrograph for simplicity. Astronomical tide and MMSL are the only predictands not simulated through the hydrographs. Instead, astronomical tides are simulated using the deterministic UTide model initialized with the pre-processed NOAA water level data (Codiga et al., 2011). MMSL was simulated using a linear regression with covariates derived from the weather types.

We implemented TESLA in Cascadia primarily using the approach developed by Anderson et al. (2019), however, there were a few differences. First, we updated the MMSL regression to include additional covariates (eq. 2). In Anderson et al. (2019), MMSL in San Diego, CA was simulated using a linear regression with just three covariates (the first three principal components (PCs) derived from the SST dataset used to produce the AWTs), producing an r-squared of 0.73. In this application, the methodology was less effective (r-squared \cong 0.57), indicating the regression was missing important drivers of water level variability in the Cascadia region. We added three additional covariates (PCs from SLP describing regional monthly averaged synoptic weather) to the approach (Mukhopadhyay et al., 2023), which improved the r-squared to \cong 0.9 in Cascadia locations.

$$\begin{split} MMSL &= a_o + a_1APC_1 + a_2APC_2 + a_3APC_3 + a_4MPC_1 + a_5MPC_2 + a_6MPC_3 \\ &+ (b_o + b_1APC_1 + b_2APC_2 + b_3APC_3 + b_4MPC_1 + b_5MPC_2 + b_6MPC_3) \cdot \cos(2\pi t) \\ &+ (c_o + c_1APC_1 + c_2APC_2 + c_3APC_3 + c_4MPC_1 + c_5MPC_2 + c_6MPC_3) \cdot \sin(2\pi t) \end{split} \tag{2}$$

Here, a, b, and c variables represent the linear regression coefficients, APCs are the AWT SST PCs, MPCs are the monthly-averaged SLP PCs, and the periodic terms serve to force an annual seasonal cycle.

A second difference from Anderson et al. (2019) is due to this being a regional (all of Cascadia), rather than local (San Diego Bay), application. Instead of building one TESLA node to drive all the waves and water levels in the Cascadia region, we built eight semi-coupled TESLA nodes at approximately one degree resolution to better capture alongshore varying conditions (fig. 3). Here, semi-coupled implies that the weather types are shared across all eight sites, while the hydrodynamic inputs and outputs, comprised of deepwater wave hindcasts, tide gauges, and simulations of those variables, are unique to each location (S1). As such, for a given TESLA simulation, large scale climate, intra-seasonality, and daily weather are consistent across the

Cascadia region, but the synthetic wave (Hs, Tp, Dir) and water level characteristics (η_{SS} , η_{MMSLA} , η_{AT}) are generated from statistical distributions based on local observations.

We created 100 hypothetical simulations of hourly future TWL drivers. Time series exploration and probability distribution functions (PDFs) of TWL drivers validate that TESLA recreates the frequency, magnitude, and timing of drivers based on statistical relationships derived from present day observations (fig. 4). From Figure 4, we see that TESLA is able to simulate both chronic and extreme conditions and can extrapolate out from observations, allowing for slightly longer tails in the synthetic distributions, while maintaining the overall distribution shape and dependencies between drivers. Coefficient of Variation (CoV), a standard technique to determine the number of simulations needed to capture a desired estimation accuracy in the modeled system (Au and Wang, 2014), indicated that 100 TESLA simulations is adequately data-rich to explore TWLs on a monthly scale (72,000 TWL data points). In this study, analyses are generally conducted on the decadal scale (>8 million data points) to explore the influence of SLR on coastal hazards. However, the number of simulations allows us to confidently explore seasonal influences on coastal hazards as well.

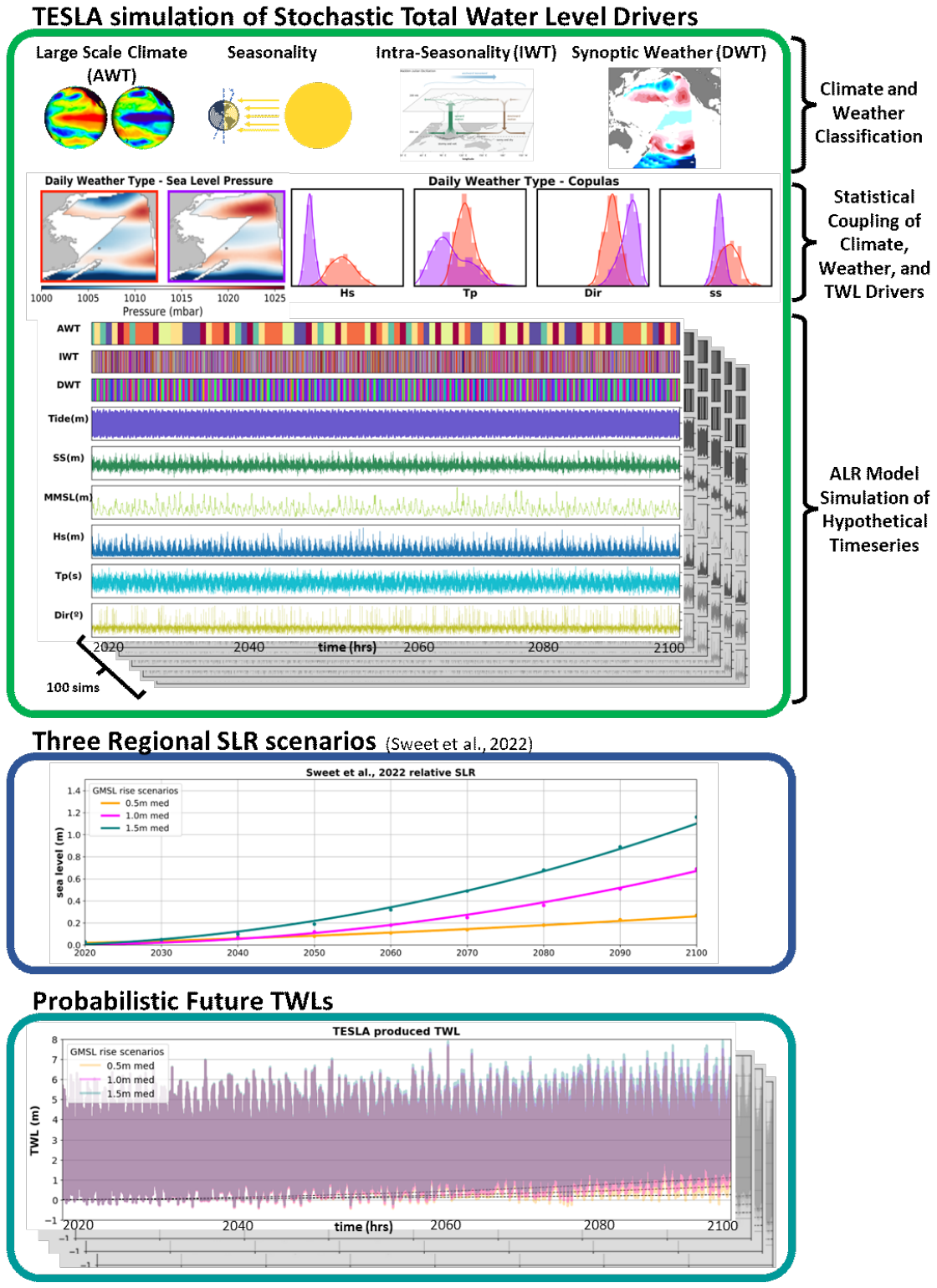


Figure 2. TESLA (Time-varying Emulator for Short- and Long-Term Analysis of flooding and erosion), a stochastic climate emulator (Anderson et al., 2019), is used to generate offshore drivers of TWLs for 2020-2100. Probabilistic TWL drivers are combined with three SLR scenarios as inputs into onshore TWL calculations.

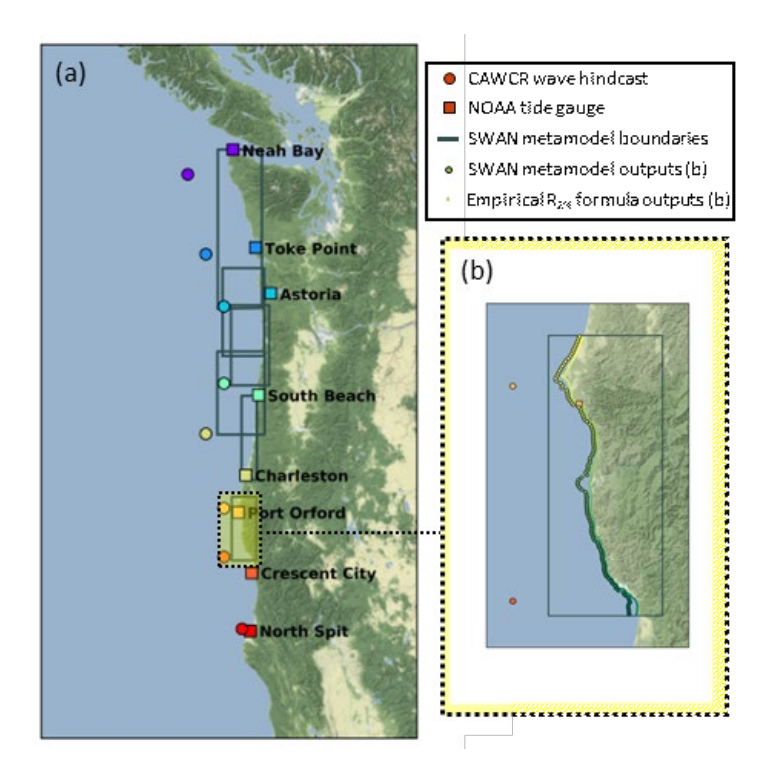


Figure 3. (a) Map of the Cascadia Region showing model inputs, domains, and resolutions. Eight semi-coupled TESLA nodes produce offshore TWL drivers at CAWCR wave hindcast locations (~1° resolution). (b) SWAN metamodels transform TESLA wave outputs to the 20m contour line (1km resolution) and empirical runup formulas calculate onshore TWLs (100m resolution)

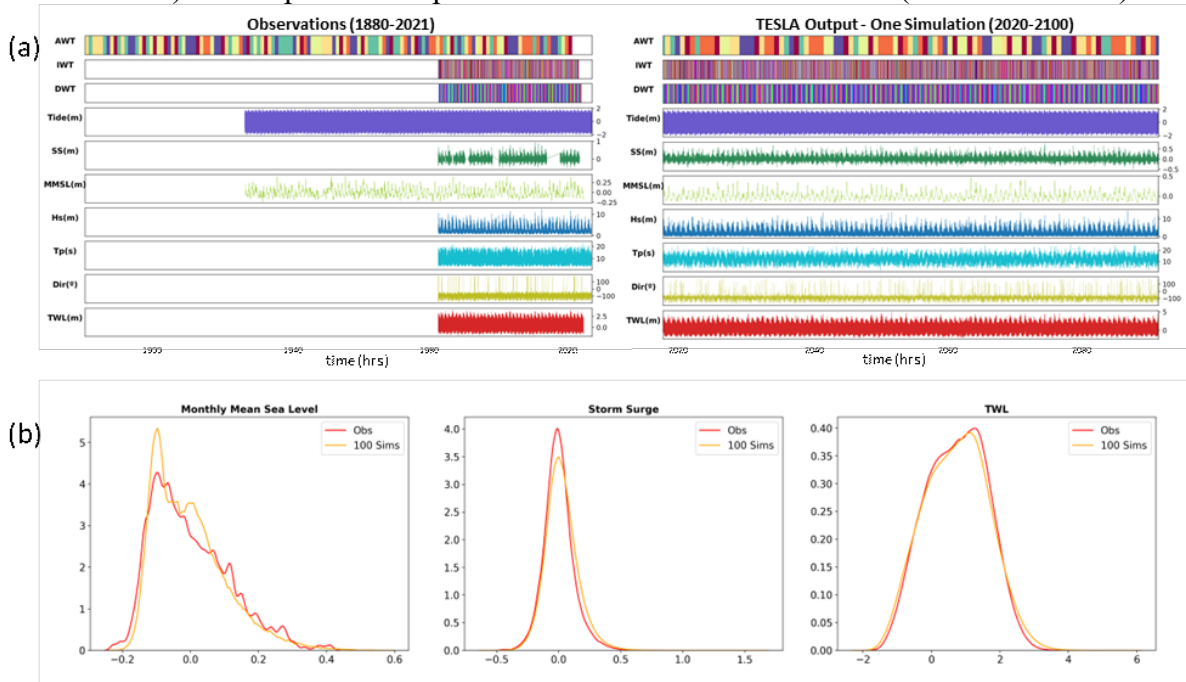


Figure 4. (a) Timeseries of TESLA inputs (observed weather types and TWL drivers) and one simulation of TESLA outputs (80 years of synthetic weather types and TWL drivers) and (b) PDFs of observed vs simulated TWL and TWL drivers for the Astoria TESLA node, demonstrating TESLA's ability to recreate present day TWL conditions.

3.1.2 Onshore Propagation of Waves

The outputs of TESLA are generated at an offshore location (the site of the wave hindcast node). To develop TWLs relevant for onshore impact assessments, TESLA outputs need to be propagated across local bathymetry and onto the beach (Serafin et al., 2019). To calculate the wave driven runup component of TWLs, we use a combination of previously developed metamodels for nearshore wave transformation (Allan et al., 2015) and empirical runup formulas. The metamodels are comprised of interpolated lookup tables generated based on stationary SWAN modeling of historical water level and wave conditions. Offshore wave simulations from TESLA are input into the SWAN lookup tables and extracted at approximately the 20m contour line at 1km alongshore resolution. They are then back propagated to compute alongshore varying effective deep-water wave conditions for input into runup models (e.g., Stockdon et al., 2006). While the surrogate models are capable of extracting waves every 100m in the alongshore direction, sensitivity testing revealed down-sampling to 1km resolution significantly reduced computational expense with low impact to final TWL values.

Using the alongshore varying wave conditions (1km resolution) and lidar-derived geomorphology (100m resolution; Shope et al., 2022) as input into empirical runup formulas, we incorporate the wave driven component of TWLs into the simulated impact analysis for the Cascadia region. Two flavors of empirical runup formulas were employed based on beach type and relative TWL elevation. The Stockdon et al. (2006) formula was applied to sandy, dune backed beaches while a modified TAW (Technical Advisory Committee for Water Retaining Structures) barrier runup method was applied to cobble, bluff, or riprap backed beaches when TWL elevation exceeded the barrier toe (Allan et al., 2015; Pullen et al., 2007; van der Meer, 2002). For sandy beaches with beach slopes greater than 0.12 we applied the barrier runup method, as the empirical data used to derive the Stockdon formula did not include such steep beaches. Headlands, estuaries, and bays were excluded from our analysis. We also excluded transects that had backshore features with unrealistic elevations (e.g., backshore feature toe >10m or crest >50m), as we assumed these reflect lidar-derived error rather than a realistic depiction of backshore features. There were two locations within our study domain that did not have existing lookup tables: in Northern California and a 30km gap in Southern Oregon. At these locations, TESLA deep water wave outputs were directly input into empirical runup formulas and no nearshore bathymetric transformation was captured. As found by Serafin et al. (2019) we expect alongshore beach topographic variability to have the largest influence on the severity of coastal impacts.

The time evolving TESLA outputs are transformed over reference bathymetry and topography that does not change over time. Nearshore bathymetric data used in the SWAN models was derived from 1/3 arc-second (~10 m) DEMs downloaded from the NOAA's National Geophysical Data Center and onshore geomorphic data is derived from a 2016 US West Coast lidar dataset (Shope et al., 2021; Shope et al., 2022). Keeping bathymetry and topography static in this analysis is a necessary choice for impact studies of this scope (100 simulations, 80 years, 9,010 transects) as existing models used for morphological evolution (e.g., XBeach, Delft3D) are largely designed for event-based simulations along a single beach (Roelvink et al., 2009). To evolve bathymetry and topography over the spatial and temporal scale of this study with available tools would therefore be computationally prohibitive and would likely yield results with unquantifiable compounding errors. It is important to note, however, that since morphology is held static, the future TWLs and hazard impact projections presented here should not be interpreted as predictions, but rather as practical projected comparisons to present day conditions.

3.2 Regional Scale Impact Analyses

We assessed the Cascadia coastline's physical exposure to extreme TWLs using three simple co-produced proxies including unsafe beach hours, collision hours, and overtopping hours. These proxies were developed from well-established coastal hazard frameworks (Sallenger, 2000) and feedback from regional stakeholders (Hadziomerspahic, 2022) (fig. 5). Collision and overtopping are classic proxies for dune face erosion and backshore flooding, respectively (Sallenger, 2000). Here we apply these metrics to dune-backed beaches in Cascadia, as well as areas with other backshore features (e.g., cliff-backed, armored, cobble beaches). While the morphological response to collision and overtopping for sandy and non-sandy coasts is different, the metrics can still indicate whether conditions that commonly lead to erosion or flooding are present.

The unsafe beach hours metric was developed through extensive engagement with stakeholders in the Cascadia region. Stakeholders highlighted that solely assessing flooding and erosion proxies tends to center hazard impact discussions on (typically wealthy) coastal property owners only. Stakeholders expressed interest in a proxy that can communicate how the general population may also be impacted by chronic coastal hazards. On their suggestion, we co-created a beach safety proxy that underscores how visitors to beaches (either for work or leisure) may feel unable to utilize the beach for their preferred activities based on its time-dependent width. To quantify beach safety, we track the number of daylight hours during which the beach is 'unsafe', or too narrow to comfortably recreate without safety concerns. The definition of 'too narrow' should be determined based on the unique conditions of a particular beach and how visitors use it. In this study a threshold width of 10m was applied regionally for simplicity after testing varying thresholds of 10m, 15m, and 20m.

Chronic Hazard Proxies

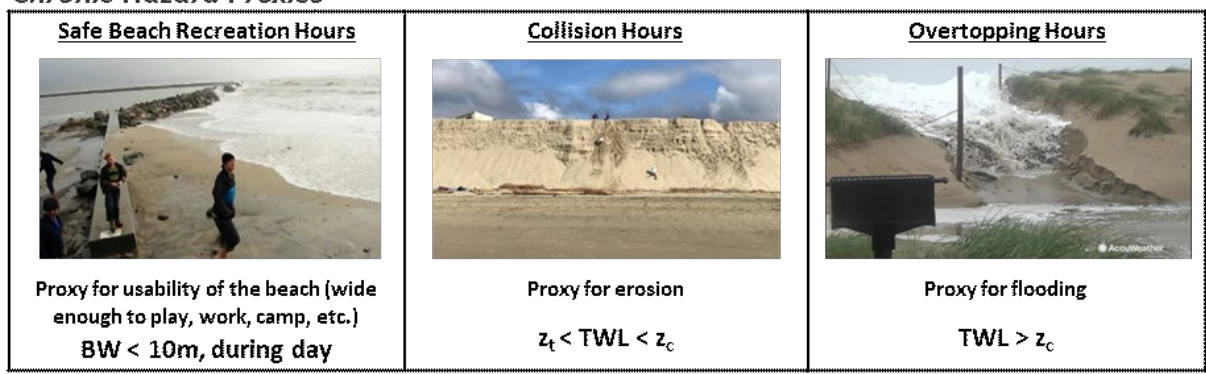


Figure 5. Description of chronic hazard proxies, where BW is the beach width, z_t is the backshore feature toe elevation, and z_c is the backshore feature crest elevation at a given transect.

We track the evolution of the hazard proxies through changes in the *percent occurrence* (eq. 3). This measurement is the sum of the total hours in which conditions for hazard impacts are met during a particular time period (impact hours) divided by the total hours in that period. Here, we largely present the percent occurrence over the duration of decades to explore the influence of SLR on hazard impacts, but different durations can be chosen based on research focus or stakeholder needs.

$$Percent \ Occurrence = \frac{impact \ hours \ during \ period}{total \ hours \ during \ period} \cdot 100 \tag{3}$$

To identify areas that experience a large change in hazard impacts compared to present day conditions, we propose a novel hotspot indicator:

$$Hotspot\ Indicator = Impact\ Multiplier \times Total\ Diff\ in\ Hours$$
 (4)

where the impact multiplier is the factor by which the hazard impact hours increase from the initial to the final timestep, and the total difference in hours is the difference in impact hours between the final time step and the initial. The combination of these two variables serves to emphasize the importance of relative change (impact multiplier), while normalizing by the total magnitude change (total difference in hours). Finally, the hotspot indicators are normalized across all metrics, and combined into a joint hazard index to produce a single hazard change score that allows for inter-site comparisons:

$$Joint \ Hazard \ Indicator = 100 * (Norm. \ Unsafe \ Hotspot * (1/3) \\ + Norm. \ Collision \ Hotspot * (1/3) \\ + Norm. \ Overtopping \ Hotspot * (1/3))$$
 (5)

4 Results

4.1 Hazard Impact Metrics at the Transect to Beach Scale

The hazard proxy impacts can be visualized at multiple spatial and temporal scales to explore the various processes influencing hazardous events. We demonstrate this by first looking at a single transect in the Rockaway littoral cell within Northern Oregon (Figure 6) and applying the percent occurrence metric (eq. 3) to the unsafe beach and erosion hazard proxies over time periods of months, years, and decades for the moderate SLR scenario (1.0m GMSLR). Flooding hazards are extremely rare at this location (occurring less than 1% of the time under all sea-level rise scenarios). However, even just a few flooding events can be extremely disruptive to communities, causing lasting closures to transportation networks and community assets. As such, low values of hourly percent occurrence for overtopping may mask the true hazard risk. For clarity, we instead present the overtopping metric as a sum of impact hours during the studied time period.

The box plots in Figure 6 show the range of variability attributable to the stochasticity of wave and water levels from the 100 TWL simulations. By assessing hazard proxy impacts over different time durations, we can see the influence of different processes (seasonality, intra-annual variability driven by weather type, intra-decadal variability driven by SLR, and variability associated with nodal cycles in the deterministic tide). The transect shown in Figure 6 lies along one of the most highly erosive stretches of beach in the Cascadia region (Light, 2021). This transect was chosen because, it's unarmored and, even amongst neighboring transects, has a relatively low dune toe elevation (3.53m) and low dune crest elevation (6.14m) allowing unsafe beach, collision, and overtopping hazards to occur more frequently than elsewhere in the region. Nevertheless, overtopping remains extremely rare throughout the 21st century under the moderate SLR scenario (median is less than 15 hrs per year in 2100). The unsafe beach proxy occurs more frequently than the erosion proxy (collision) because anytime the total water level is high enough to trigger a collision or overtopping hazard the beach will also have a width less than 10m. At this transect, beach safety also tends to have more variability across the simulation space than the erosion proxy (collision) as seen by the size of the box body and whiskers, particularly when looking at percent occurrence over shorter durations. This could be explained by the relatively shallow slope at this beach, which allows small variations in TWL height to drastically affect beach width. Both the unsafe beach metric and collision metric almost triple in percent occurrence over the 80-year

simulations for the 1.0 m SLR scenario (median unsafe beach increases from 17% to 46%; median collision increases from 15% to 45%).

In Figure 7, we show a similar analysis, but have increased the number of transects to 50 (~5km of coastline) to explore how morphology as well as TWL stochasticity can influence hazard occurrence. In this stretch of coast, only five transects are armored with riprap, the rest are sandy dune backed. The morphology of this stretch averages to slightly steep beaches (slope=0.04) and moderate backshore feature elevations (z_t =5.5m, z_c =6.1m). However, there are a few transects with very steep beaches (slope>0.10) and low dune toes (>4m). In this analysis, morphologic features like dune toe elevation, dune crest elevation, and beach slope are significant controls on the time evolution and variance of hazard occurrence. As these transects on average have dune features at higher elevations than the single transect analyzed in figure 6, the three hazard proxies occur with less frequency. Incorporating morphological variability into the percent occurrence analysis tends to dramatically lower the box bodies (interquartiles). At the transect explored in figure 6, unsafe beach and collision hazards occur over 15% of the time in the median case during 2020. Incorporating neighboring transects into this analysis lowers the 2020 median percent occurrence to less than 5%, indicating that even along this notoriously erosive stretch of beach, most transects spend relatively little time experiencing hazardous conditions. Similarly, the overtopping hazard box bodies shrink while the whiskers (i.e., the extremes, 0.05 and 0.95 quantiles) lengthen, further demonstrating that in this 5km stretch, a few transects are responsible for extreme overtopping conditions and the rest of this area's morphology is fairly similar. This serves to narrow the body of the distribution of hazard percent occurrence, while lengthening the tails.

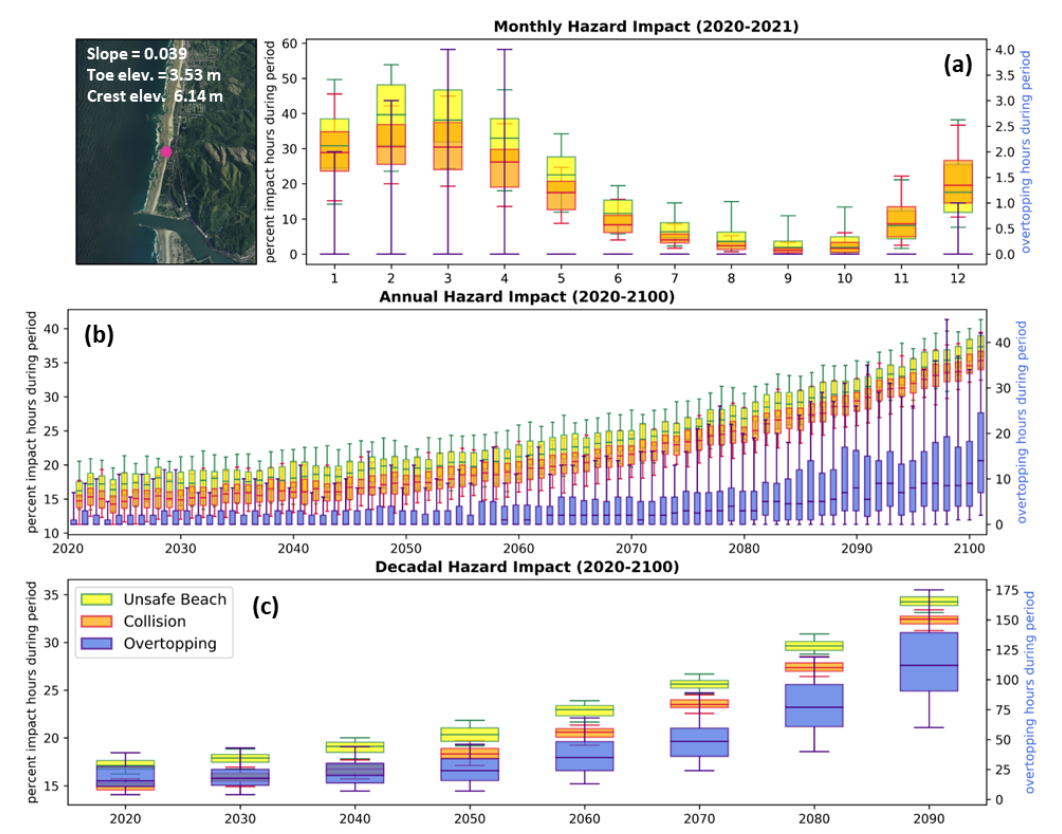


Figure 6. Box plots of percent occurrence (or total impact hours) for the three impact metrics during 100 simulations of TWL under the 1.0m GMSLR scenario, calculated over different time durations at a single transect. Box plot bodies represent 0.75 and 0.25 quantiles, whiskers represent 0.05 and 0.95 quantiles, and lines within the box body represent the median hazard percent occurrence value. The percent occurrence captures seasonal (a), interannual (b), or interdecadal (c) evolution of hazard metrics depending on the duration explored, box plot bodies and whiskers show the range of hazard variability produced by probabilistic simulations of TWLs.

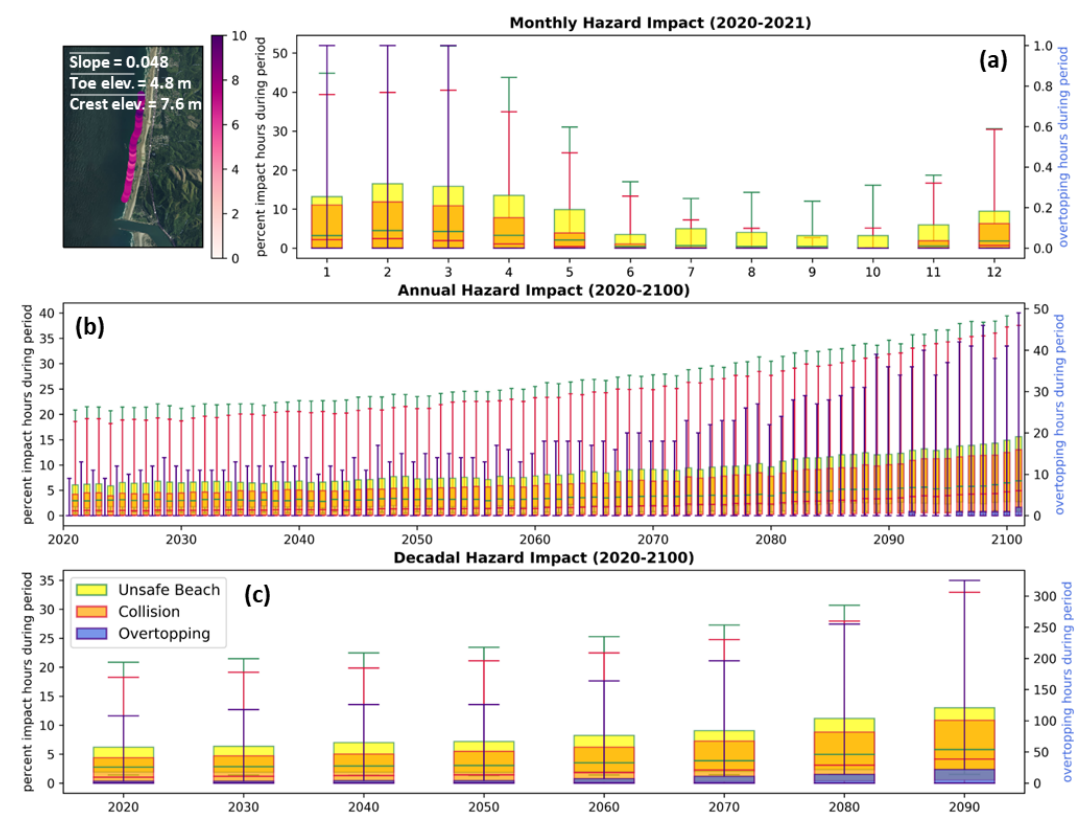


Figure 7. Box plots of percent occurrence for the three impact metrics during 100 simulations of TWL under the 1.0m GMSLR scenario, calculated over different time durations at 50 transects over a 5 km stretch of coast. Average morphology is shown on the map, with colored dots indicating toe elevation at each transect. Box plots show the range of hazard variability when both probabilistic water levels and static geomorphology are included in the analysis. Variability in local geomorphology lowers interquartiles (box bodies) of hazard percent occurrence, while lengthening the extremes represented by the 0.05 and 0.95 quartiles (whiskers).

4.2 Hazard Impact Metrics at Regional Scale

For the regional scale analysis, it was necessary to simplify the dimensionality of the simulation space before analyzing hazard impacts to retain computational efficiency. To do this, we saved the hourly median (0.5) and tails (0.05 and 0.95) of the distribution representing how likely it was for a hazard impact to occur over the 100 simulations using binomial maximum likelihood estimates (MLE). These three likelihood estimates are used to approximate the hazard probability space without calculating the full probability distribution at every transect on the regional scale. After calculating the hourly likelihood, we explored hazard impacts over our different time periods of interest. Regional scale results for 0.05, 0.50, and 0.95 probabilities are presented below; more detail on this methodology can be found in the supplemental section (S2).

In figure 8, we present the median probability percent occurrence for the last decade of the 21st century (2090-2100) under 'no SLR', low, medium, and high RSLR scenarios, calculated at each transect and then averaged over the littoral cell scale (ranging from ~10km to 50km). This offers a comparison of hazards one could expect during hypothetical simulations of present day mean sea level to those they could expect under the three SLR scenarios. While averaging over the littoral cell scale obfuscates extremes caused by morphological variability on a transect by

transect basis, it allows for first cut identification of coastal communities that may experience disproportionate hazard exposure. Averaging over the entire Cascadia region and using the 0.5 MLE, unsafe beach conditions occur between 12-21% of the time by 2100 dependent on the sealevel rise scenario explored. Collision (erosion) conditions occur between 10-19% of the time. Under all sea-level rise scenarios, overtopping (flooding) remains rare (<1%), occuring just a few times per year. However, as noted above, a few hours of flooding can be catastrophic, and just 0.5% percent occurrence of overtopping translates to 438 hours of flooding in a decade. As such, low values of hourly percent occurrence for overtopping may mask the true hazard risk and should be interpreted carefully.

While the heat maps in figure 8 (and fig. 9) provide information on average hazard severity in a littoral cell, they don't reveal where the individual transects that experience the most extreme hazard impacts are located. We identified transects with 'extreme' hazards as those that exceed the top 10th percentile of hazard impacts over the region for a given period. During 2090-2100, transects that exceed 139 (daylight) days/year of unsafe beaches, 238 days/year of erosional conditions, or 3.8 hours/year of flooding fall within the top 10th percentile. Figure 10 shows the percentage of transects in a littoral cell that are in the top 10th percentile. Transects that experience the most extreme unsafe beach hazards are concentrated in Northern Cascadia along the Olympic Peninsula, where mixed sediment beaches, steep beach slopes, and low backshore feature toes lead to narrower beach widths (fig. 11). For collision and overtopping, there are higher concentrations of top 10% transects in both Southern and Northern Cascadia, where mixed sediment bluff backed beaches have relatively low backshore feature toes and crests.

After exploring the median (0.5 MLE) cases in figures 8 and 10, we quantify the uncertainty associated with TWLs for each hazard under one SLR scenario (fig. 9) by comparing the 0.95 and 0.05 MLEs to the median. Uncertainty varied spatially, temporarily, and by hazard. Spatially, uncertainty is fairly uniform across SLR scenarios for overtopping hazards. However, for unsafe beach and collision hazards there is slightly higher hazard uncertainty in southern Cascadia and northern Washington than the rest of the region. This spatial pattern is consistent through time and across SLR scenarios, and correlates strongly with on average steeper beach slopes (~0.10) and a high proportion of mixed sediment bluff backed beaches (fig. 11).

Temporally, TWL-derived uncertainty increases linearly across the entire region between 2020 and 2100. By the end of the century, the TWL uncertainty, calculated by subtracting the 0.05 MLE from the 0.95 MLE and averaging over the region and the three SLR scenarios, is 8.3%, 6.6%, and 3.7% for unsafe beach, collision, and overtopping hazards, respectively. The hazard uncertainty derived from SLR scenarios increases exponentially throughout the century. By 2100, the uncertainty range associated with SLR scenarios for unsafe beach and collision hazards is similar to the average TWL-induced uncertainty (8.7%, 8.4%), but much lower than the TWL-induced uncertainty for overtopping hazards (0.3%). It is only in the last decade of the century that uncertainty associated with the three SLR scenarios exceeds the uncertainty derived from stochastic TWL variability for any of the hazards.

Hazard uncertainty has a non-normal distribution, with long tails skewed towards more hazardous events, i.e., the difference between the 0.95 quantile and the 0.50 quantile exceeds the difference between the 0.50 and 0.05 quantiles. This pattern is similarly seen in the box plots of figure 7, where hazard percent occurrence 'bottoms out', limiting the uncertainty range between low and median quantiles, but often capturing very high variability at the 0.95 quantile based on morphology.

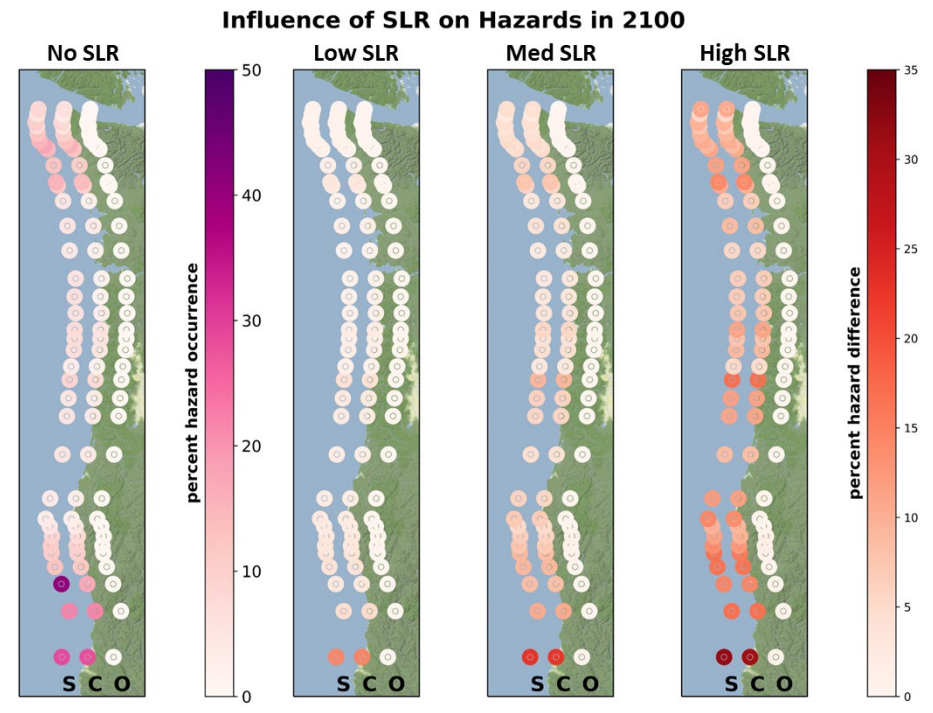


Figure 8. Median percent occurrence of unsafe beach conditions (S), collision conditions (C), and overtopping conditions (O) during 2090-2100 decades under a 'no SLR' scenario (purple colorbar) and the difference between 'no SLR' and low (0.5m), medium (1.0m), and high (1.5m) SLR scenarios (red colorbar) averaged over littoral cells.

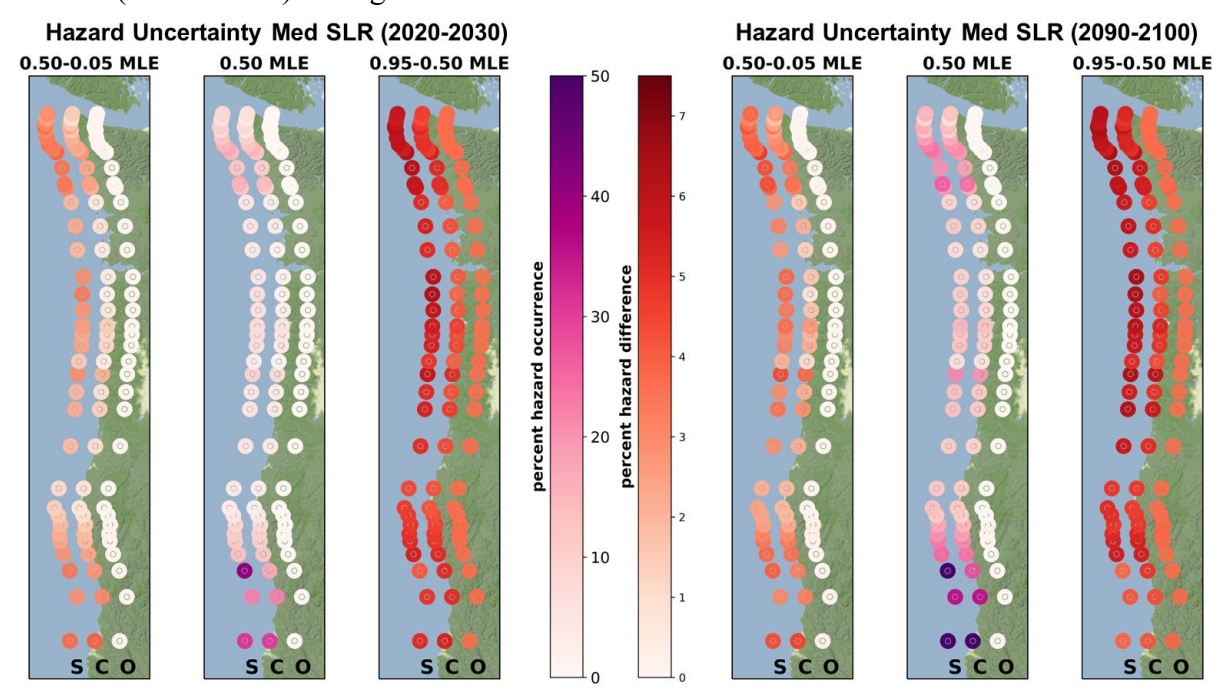


Figure 9. Difference between median hazard percent occurrence (middle panels, purple colorbar on left) and 0.05 (left panels, red colorbar) and 0.95 (right panels, red colorbar) MLEs caused by variability in wave and water level drivers in the decades beginning in 2020 and in 2090 under the medium (1m GMSLR) scenario for unsafe beach conditions (S), collision conditions (C), and overtopping conditions (O).

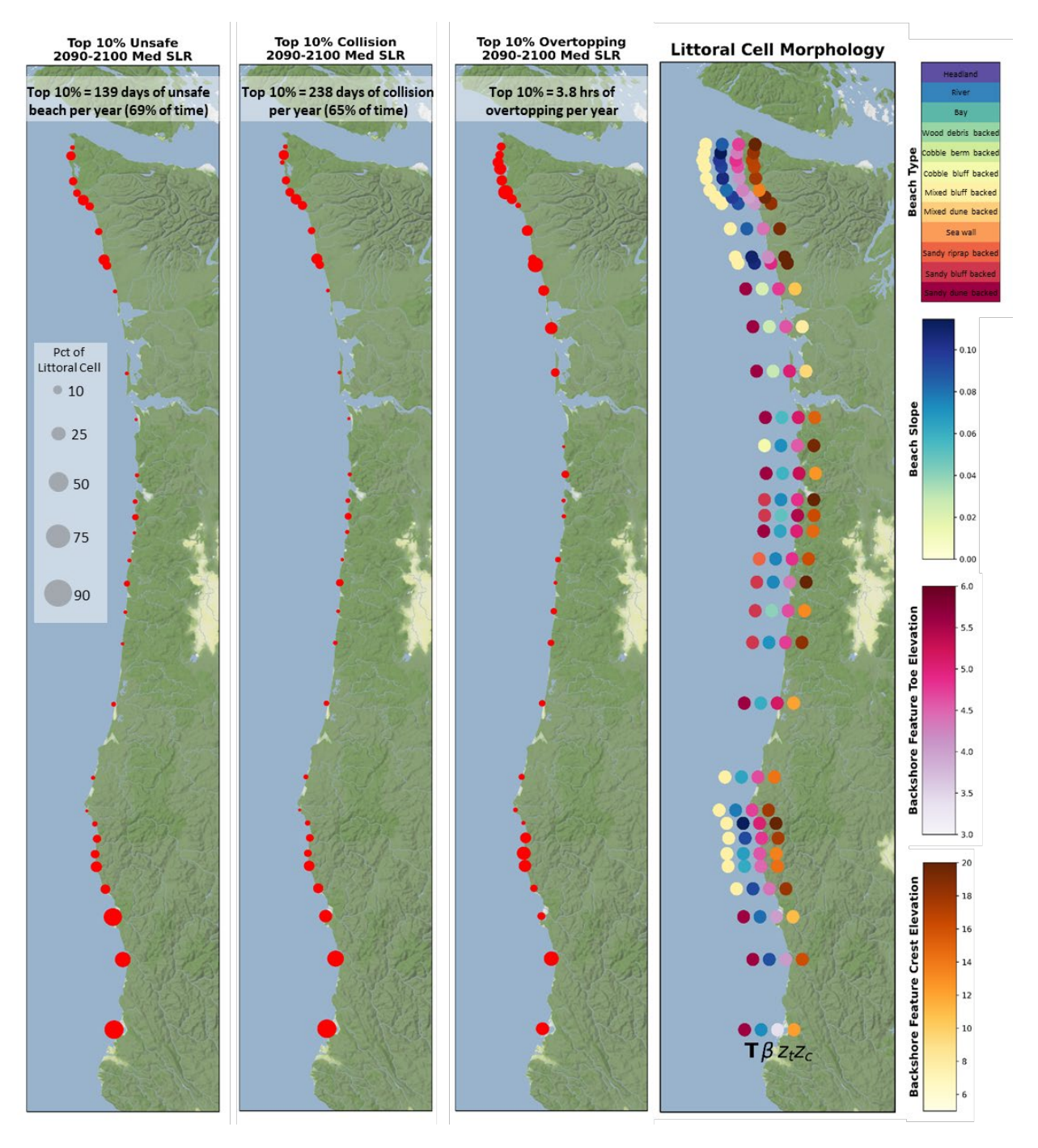


Figure 10. Percentage of transects in each littoral cell that exceed the 10th percentile of hazard impact during 2090-2100 under the 0.5MLE and median SLR scenario.

Figure 11. Median beach type and average morphology for each littoral cell in the Cascadia Region, where T is beach type, β is beach slope, z_t is backshore feature toe elevation, and z_c is backshore feature crest elevation.

4.3 Hazard Change Hotspots

Hotspots of hazard change in the Cascadia region were identified using the Hotspot Indicator (eq. 4) and the Joint Hazard Change Indicator (eq. 5). Figure 12 depicts both indicators, with the Joint Hazard Change Indicator represented by the size of each pie chart (areas with larger pie charts will see high increases in hazard occurrence from the initial decade (2020-2030) to the final decade (2090-2100) in our analysis). The slices of the pie chart reveal the individual contributions of the Hotspot Indicators (increase of a single hazard proxy) to the overall Joint Hazard Change Indicator. As expected, the highest increase in hazards occurred under the largest SLR scenario explored. Unsafe beach and erosion hazards are the dominant contributors to the joint hazard change in the Cascadia region during the 21st century. Only under the high SLR scenarios and in specific areas of the Cascadia region do overtopping hazards begin to significantly influence the hazard change indices. The areas that experience large changes in overtopping also have the greatest joint hazard change. Overtopping increases most in Southern Cascadia (Southern Oregon and Northern California) and parts of Northern Cascadia (Washington). Many of these littoral cells are the same areas marked by large numbers of extreme (top 10th percentile) hazard transects and higher hazard uncertainty. Erosion (collision), across all sites and sea-level rise scenarios, is the greatest contributor to the joint hazard indicator. Its influence on the joint hazard indicator increases as the SLR scenario grows. While unsafe beach hazards also continue to increase through SLR scenario, the rapid change in erosion hazards leads to a relative reduction in the unsafe beach hazard contribution to the overall joint hazard change.

Areas of greatest joint hazard change are focused around the southern portion of the Cascadia Region and around the mouths of estuaries in Southern Washington and Northern Oregon (Columbia River and Willapa Bay) and in Central Oregon (Yaquina Bay). In Southern Cascadia, this joint hazard increase is again correlated to the presence of mixed sediment bluff backed beaches and low backshore feature elevations. Around the estuaries, the joint hazard increase seems associated with relatively shallow beach slopes and low backshore feature elevations (toes in Oregon and both toes and crests in Washington), allowing for small changes in TWL to significantly increase the occurrence of all hazard proxies. Notably, some of the littoral cells that have the greatest increase in joint hazard change do not have a large proportion of transects in the top 10th percentile of hazard impacts.

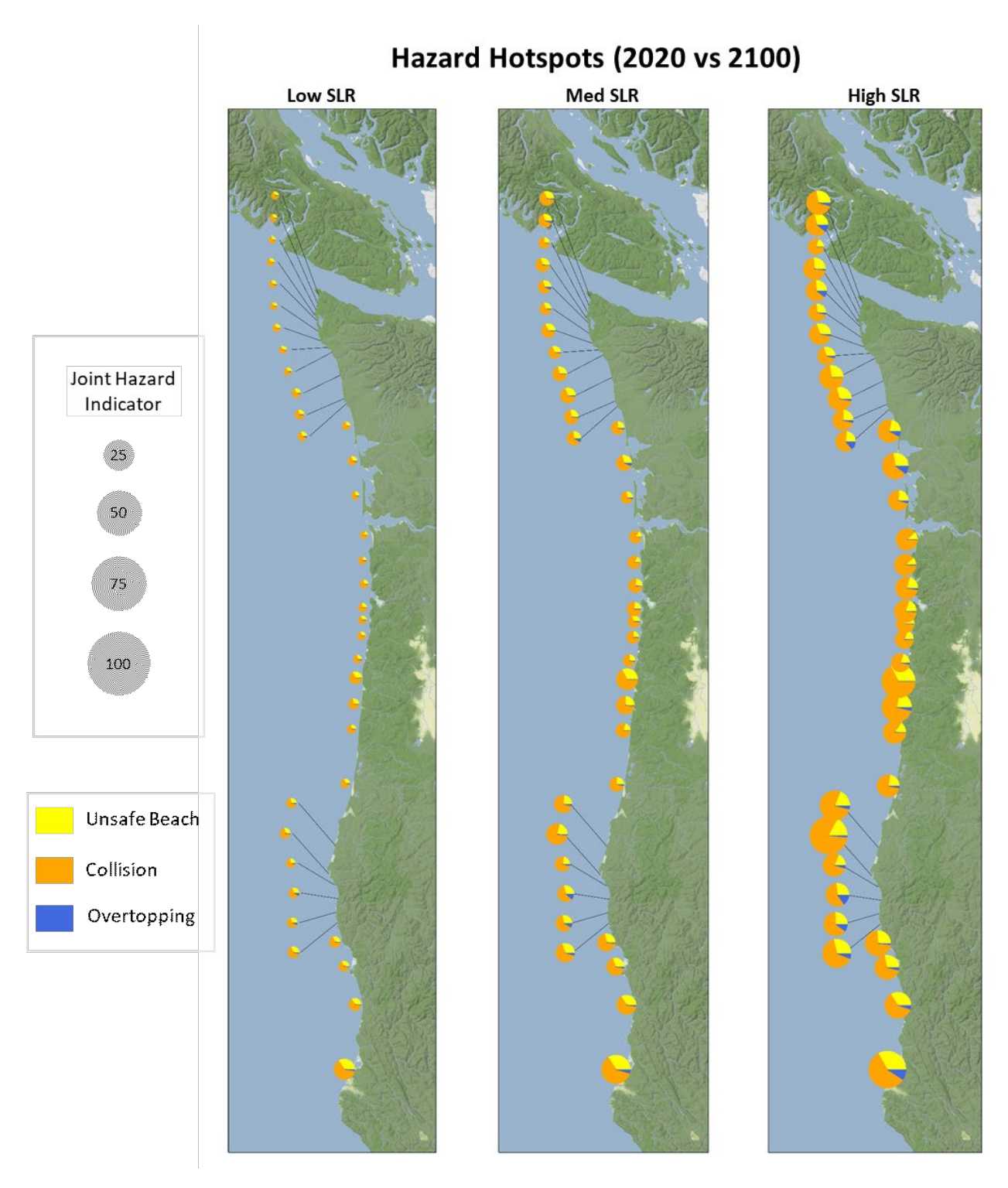


Figure 12. Hazard change hotspots from 2020-2100 under three SLR scenarios. The size of the pie charts is determined by the Joint Hazard Change Indicator, while the individual contributions of the Hazard Hotspot Indicators to the Joint Hazard Change Indicator make up the pie chart slices.

5 Discussion

5.1 Hazards and Hazard Change Hotspots

Computing simple hazard proxies enables stochastic hazard analysis over large spatial (950 km) and temporal (80 year) scales. They are fast to compute yet maintain relatively high resolution (100m-1,000m scale). They offer valuable comparisons to present day conditions while generating quantitative results that affected coastal communities have identified as critical for their hazard planning efforts. The hazard proxies and hazard change indices chosen for this study were the result of extensive co-production, so results fill stated needs of Cascadia's coastal planners while simultaneously progressing fundamental knowledge about how chronic coastal hazards will evolve under climate change.

This study produces probabilistic estimates of hazard impact and hazard change in the Cascadia region. Under the low SLR scenario (0.5m GMSLR), median likelihood case for TWL variability, littoral cells in the Cascadia region will have a less than 3% increase in unsafe beach and erosion hazard percent occurrence by the end of the century and a less than 0.05% (~44 hours per decade) increase in flooding. Under the medium (1.0m GMSLR) and high SLR scenarios (1.5m GMSLR), Cascadia on average will experience an additional 5% and 10% increase in unsafe beach and collision percent occurrences for the respective scenarios. Under those same scenarios, the Cascadia region will on average increase flooding by approximately 115 and 270 hours by the end of the century. This indicates that the Cascadia region must prepare for a wide range of hazard evolution under different sea-level rise scenarios.

Coastal flooding is projected to remain rare in Cascadia, even under the most severe SLR scenarios, occurring less than 0.5% of the time in 2090-2100. This aligns with current knowledge about the Cascadia region, as most outer coast beaches in the region are dominated by relatively tall, linear dunes or bluffs that offer protection from flooding. However, while most of the Cascadia coast will remain resistant to flooding hazards, projections indicate that several low-lying areas in Cascadia will bear the brunt of vulnerability (fig. 10). In these areas, rare flooding events have the potential to be extremely costly, damaging infrastructure and disrupting transportation networks beyond the perceived area of impact.

This study also identifies hotspots of hazards, areas that are expected to face larger changes in hazard exposure during the 21st century than their neighbors. Cascadia region stakeholders have stated that identifying areas of large hazard change is of high priority. Areas that rarely or never experience a hazard under present-day conditions but will experience an increase in the future may be under-prepared for climate change induced hazards. These communities currently experience no incentive to prepare for changing conditions due to a historical sense of security. They therefore may be the most impacted and ill-equipped for coping with increasing hazards (Thompson et al., 2023). Areas of hotspot change may also be the best candidates for climate-informed planning, as they may require relatively little investment to carry out proactive adaptation rather than being forced to respond to hazards in real time. Overtopping in particular does not increase dramatically throughout the region, except for a few littoral cells under the most extreme SLR scenario. Dedicating adaptation resources to these hotspot areas in advance may mitigate extensive longterm costs (financial and social). Furthermore, some of the areas that have a large joint hazard change do not contain a large proportion of transects in the top 10th percentile of hazard impacts (e.g., in central Oregon). This highlights the need to explore not just total hazard impact, but the rate of hazard change. The hotspot indicators and joint hazard indicators were designed to provide stakeholders with simple, comparative, tools that highlight areas that experience dramatic changes in hazard conditions under different climate change scenarios.

Our analysis indicates that littoral cells in southern Cascadia and around the mouths of large estuaries are likely to experience the greatest joint hazard change. Across almost all littoral cells and sea-level rise scenarios, the collision hazard proxy increases the most between 2020 and 2100. However, a few regions will also experience large increases in flood hazards. The spatial variability in hazard percent occurrence and hazard change is strongly correlated to beach morphology (beach type, beach slope, and backshore feature elevation). This indicates that there is potentially high under preparedness for erosional hazards across the entire Cascadia region and flooding hazards in select littoral cells. Local scale case studies to identify where these hazards are focused and who they impact (e.g., are valuable community assets exposed? what is adaptive capacity in this region?) are necessary to determine whether adaptation efforts should be of higher priority in these areas compared to areas that will see smaller rates of hazard evolution.

5.2 Drivers of Chronic Coastal Hazards and Hazard Uncertainty in the Cascadia Region

The probabilistic nature of this analysis provides new insights into how variability in wave and water level drivers translates into uncertainty of hazard impacts. Hazard uncertainty increases over time and for higher sea-level rise scenarios. Unsafe beach and erosion hazards have fairly similar uncertainties when averaged over the entire Cascadia region. There is slight spatial variability in hazard uncertainty, which correlates with morphologic characteristics in the region, particularly mixed sediment bluff backed beaches in Southern Cascadia. This corresponds well to Serafin et al.'s (2019) finding that local bathymetry and beach morphology are dominant controls in determining onshore impacts of extreme TWLs. They found that the bathymetric and morphologic setting can cause large, nonlinear changes to impact hours experienced by the backshore with only small variations in TWLs. In probabilistic simulations of TWLs, small variations in water level elevations can translate to high uncertainty in hazards.

Our analysis also shows that throughout the 21st century, probabilistic TWL variability is a greater or equal contributor to hazard uncertainty than the low, medium, or high median RSLR scenarios. This indicates that Cascadia region chronic coastal hazard assessments and hazard adaptation plans must incorporate TWL variability into their frameworks to accurately evaluate near future hazard risk and uncertainty.

5.3 Implications of Hazard Proxies for Cascadia Communities and Ecosystems

While hazard proxies provide a probabilistic range of potential impacts in comparison to present day hazard conditions, how these proxies translate to vulnerability, landscape change, and ecosystem services is challenging to quantify, particularly when accounting for the various adaptation strategies communities might employ.

The combination of intensifying hazards and adaptation decisions also has large implications for tipping points or thresholds in coastal systems. Thresholds could be defined in a physical sense (e.g., endangered species habitat loss, a dune's ability to recover) or in a social sense (e.g., how much flooding/ erosion/ beach narrowing is a community willing to tolerate). While it's difficult to apply hazard proxy analysis to quantitatively predict physical tipping points, probabilistic hazard proxies may be useful for communities in establishing social thresholds and setting goals for 'bounce forward' rather than 'bounce back' hazard adaptation.

5.4 Validity of Assumptions, Areas of Future Research, and Applicability to Other Regions

While in this application we account for daily (synoptic weather), intra-seasonal (MJO), seasonal, and interannual (ENSO) variability, at the decadal- to century-scale we assume that there is stationarity in the climate, weather, and hydrodynamic drivers of total water levels. As implemented here, TESLA relies on observations of oceanographic and atmospheric variables to recreate the statistics of present day chronic and acute conditions through weather typing. Although there is growing evidence of non-stationarity in waves and water levels under a changing climate (Erikson et al., 2022), there is still high uncertainty surrounding how climate change, beyond SLR, will influence the phenomena that drives TWL variability (Morim et al., 2023). As such, we chose to investigate the probability range of TWLs and hazard impacts associated with the statistics of the present-day wave and water level climate. As knowledge of future non-stationarity is refined and global climate model outputs become more sophisticated, TESLA is capable of incorporating this knowledge by tuning the behavior (timing, duration, and intensity) of its weather types. Future work could compare simulations of TWL and hazard impact under assumptions of stationarity or non-stationarity.

This study produced a highly unique dataset (probabilistic TWLs and hazard proxies for the 21st century at 100m resolution over greater than 900 km). As such, several research pathways can leverage the publicly accessible data for their own work including hydrodynamic flood modeling, shoreline change modeling, estuary evolution modeling, etc. One research pathway Cascadia stakeholders highlighted is a significant need for coastal hazard equitable resilience studies focused on climate change induced hazards. Most existing studies that explore differential community vulnerability to coastal hazards in the Cascadia region focus on tsunami and earthquake hazards (e.g., Wood et al. 2010; Stanton et al., 2022). Future work could tie the chronic hazard proxies explored here to assessments of coastal vulnerability and adaptive capacity to help improve community understanding of which populations may need more resources to adapt to climate change.

Finally, while this study focuses on the Cascadia region, there is broader applicability. The coastal hazard proxy framework and hotspot change indices presented here can be applied on any coastline with projections of future TWL data. Furthermore, broader connections between chronic coastal hazards and drivers may also be inferred. Stochastic TWL variability causes hazard uncertainty greater than or equal to the uncertainty caused by median SLR scenarios throughout the 21st century. Coastal hazard impacts, hazard change rates, and hazard uncertainty have high correlation to morphology.

6 Conclusions

This study presents an assessment of probabilistic chronic coastal hazards in the Cascadia USA region from 2020-2100 using three simple hazard proxies for unsafe beaches, coastal erosion, and flooding and novel indices to identify areas of large hazard change. Beaches in Southern Cascadia and in the Olympic Peninsula of Northern Cascadia have the highest concentration of top 10th percentile hazard impact transects, due to their morphologic setting. These areas, dominated by mixed sediment bluff backed beaches (Southern Cascadia) and low elevation backshore features (around the mouths of estuaries), additionally tend to experience greater rates of hazard change. Collision (erosion) hazards will increase the most of the three proxies explored during the next century, indicating coastal communities in Cascadia may have the opportunity to mitigate large erosional impacts should there be concentrated adaptation efforts

dedicated to this hazard. We found hazard proxy uncertainty to have a non-normal distribution, particularly for the erosion and overtopping proxies, with the distributions having longer tails for extreme (0.95 likelihood) impacts and 'bottoming out' for median and low (0.05) likelihood cases. This analysis reveals new insights into the drivers of chronic coastal hazards in the Cascadia region and presents hazard change assessment tools that could be extended to new locations. This study further provides a hazard assessment on spatial and temporal scales relevant to management timelines and guided by a community based advisory council.

Acknowledgements

Global wave hindcast data is accessible on the Centre for Australian Weather and Climate Research (CAWCR) website. Tide gauge records are available on the National Oceanographic and Atmospheric Administration (NOAA) and US West Coast lidar-extracted morphologic data is available through the USGS. We thank James Shope (Rutgers Climate Institute) for supplementing morphologic data available online with beach slopes and labeled beach types. We also thank Jonathan Allan (Oregon Department of Geology and Mineral Industries) and Rajasree Bharathan (Oregon State University) for providing beach type data for the state of Oregon. Lastly, we extend our sincere thanks to members of our advisory council for their generosity in sharing their time and expertise over the last 5 years.

We acknowledge funding that supported this research in part from Oregon Sea Grant under Award NA18OAR170072 (CDFA 11.417) from the National Oceanic and Atmospheric Administration's National Sea Grant College Program, from the Cascadia Coastlines and Peoples Hazards Research Hub, an NSF Coastlines and People Large-Scale Hub (NSF award number 2103713), and from NOAA via the NOS/NCCOS/CRP Effects of Sea-Level Rise (ESLR) Program (award number NA19NOS4780180). Additional funding was also provided by the Juan de la Cierva – Formación FJC2021-046933-I/ MCIN/ AEI/ 10.13039/501100011033 and the European Union "NextGenerationEU"/ PRTR.

CRediT authorship contribution statement

Meredith Leung: Conceptualization, Methodology, Software, Validation, Formal analysis, Data Curation, Writing - Original Draft, Visualization

Laura Cagigal: Methodology, Software, Data Curation, Writing - Review & Editing

Fernando Mendez: Conceptualization, Methodology, Writing - Review & Editing

Peter Ruggiero: Conceptualization, Methodology, Resources, Writing - Review & Editing, Supervision, Project administration, Funding acquisition

Open Research

Models and visualization tools used in this paper were developed in Python Jupyter notebooks and in Matlab. Model codes and data visualization notebooks for the Cascadia region application of TESLA are hosted on GitHub (https://github.com/meredithleung/teslakit-cascadia). Data used in study include NCEP Climate Forecast System Reanalysis (CFSR) and Extended Reconstructed Sea Surface Temperature Version 4 (ERSSTv4) datasets, which are freely available

through NOAA/NCAR, Boulder, Colorado, USA, from their website at https://rda.ucar.edu/datasets. Madden-Julian Oscillation EOFs were downloaded from the Australian Bureau of Meteorology at www.bom.gov.au/climate/mjo. Wave hindcasts are available through the Centre for Australian Weather and Climate Research (CAWCR) at https://data.csiro.au/collection/csiro:39819 and tide gauge data were downloaded from NOAA (https://tidesandcurrents.noaa.gov/). Data produced from this analysis (e.g., TWL timeseries) will be hosted on DesignSafe (https://www.designsafe-ci.org/) by the time of publication.

References

- Allan, J., Ruggiero, P., García Medina, G., Harris, E., Roberts, J., & Stimely, L. (2015). Coastal flood hazard study, Clatsop County, Oregon. https://doi.org/10.13140/RG.2.1.1656.5608
- Anderson, D., Rueda, A., Cagigal, L., Antolinez, J. A. A., Mendez, F. J., & Ruggiero, P. (2019). Time-Varying Emulator for Short and Long-Term Analysis of Coastal Flood Hazard Potential. Journal of Geophysical Research: Oceans, 124(12), 9209-9234. https://doi.org/10.1029/2019jc015312
- Anderson, D., Ruggiero, P., Mendez, F. J., Barnard, P. L., Erikson, L. H., O'Neill, A. C., . . . Marra, J. (2021). Projecting Climate Dependent Coastal Flood Risk With a Hybrid Statistical Dynamical Model. Earth's Future, 9(12). https://doi.org/10.1029/2021ef002285
- Anderson, J.K. (2018)., "Sea-Level Rise in the Humboldt Bay Region Update 2." Local Reports and Publications. Humboldt State University. Retrieved from: https://digitalcommons.humboldt.edu/hsuslri_local/5
- Antolínez, J. A. A., Méndez, F. J., Camus, P., Vitousek, S., González, E. M., Ruggiero, P., & Barnard, P. (2016). A multiscale climate emulator for long-term morphodynamics (MUSCLE-morpho). Journal of Geophysical Research: Oceans, 121(1), 775-791. https://doi.org/10.1002/2015jc011107
- Ardhuin, F., O'Reilly, W. C., Herbers, T. H. C., & Jessen, P. F. (2003). Swell Transformation across the Continental Shelf. Part I: Attenuation and Directional Broadening. Journal of Physical Oceanography, 33(9), 1921-1939. https://doi.org/https://doi.org/10.1175/1520-0485(2003)033<1921:STATCS>2.0.CO;2
- Atwater, B. F. (1987). "Evidence for Great Holocene Earthquakes Along the Outer Coast of Washington State." Science 236(4804): 942-944. doi:10.1126/science.236.4804.942
- Au, S. K., and Wang, Y. (2014). Engineering risk assessment with subset simulation, Wiley, Chichester, U.K.
- Barnard, P. L., Short, A. D., Harley, M. D., Splinter, K. D., Vitousek, S., Turner, I. L., . . . Heathfield, D. K. (2015). Coastal vulnerability across the Pacific dominated by El Niño/Southern Oscillation. Nature Geoscience, 8(10), 801-807. https://doi.org/10.1038/ngeo2539
- Barnard, P. L., Hoover, D., Hubbard, D. M., Snyder, A., Ludka, B. C., Allan, J., . . . Serafin, K. A. (2017). Extreme oceanographic forcing and coastal response due to the 2015–2016 El Niño. Nature Communications, 8(1), 14365. https://doi.org/10.1038/ncomms14365

- Barros, V., Mastrandrea, M., Abdrabo, M., Adger, W., Federation, Y., Anisimov, O., . . . Yohe, G. (2014). Climate change 2014: impacts, adaptation, and vulnerability IPCC WGII AR5 summary for policymakers. In (pp. 1-32).
- Biel, R. G., Hacker, S. D., Ruggiero, P., Cohn, N., and Seabloom, E. W.. (2017). Coastal protection and conservation on sandy beaches and dunes: context-dependent tradeoffs in ecosystem service supply. Ecosphere 8(4):e01791. 10.1002/ecs2.1791
- Bond, H. (2021). Guidebook on Erosion Control Practices of the Oregon Coast, Oregon Department of Land Conservation and Development (DLCD). Retrieved from https://www.oregon.gov/lcd/Publications/guidebook erosion control practices.pdf
- Boumis, G., Moftakhari, H. R., & Moradkhani, H. (2023). Coevolution of Extreme Sea Levels and Sea-Level Rise Under Global Warming. Earth's Future, 11(7), e2023EF003649. https://doi.org/https://doi.org/10.1029/2023EF003649
- Burgette, R. J., Weldon, R. J., & Schmidt, D. A. (2009). Interseismic uplift rates for western Oregon and along-strike variation in locking on the Cascadia subduction zone. Journal of Geophysical Research: Solid Earth, 114(B1). https://doi.org/10.1029/2008jb005679
- Cabana, D., Rölfer, L., Evadzi, P., & Celliers, L. (2023). Enabling Climate Change Adaptation in Coastal Systems: A Systematic Literature Review. Earth's Future, 11(8), e2023EF003713. https://doi.org/https://doi.org/10.1029/2023EF003713
- Cagigal, L., Rueda, A., Anderson, D., Ruggiero, P., Merrifield, M. A., Montaño, J., . . . Méndez, F. J. (2020). A multivariate, stochastic, climate-based wave emulator for shoreline change modelling. Ocean Modelling, 154. https://doi.org/10.1016/j.ocemod.2020.101695
- Callaghan, D. P., Nielsen, P., Short, A., & Ranasinghe, R. (2008). Statistical simulation of wave climate and extreme beach erosion. Coastal Engineering, 55(5), 375-390. https://doi.org/10.1016/j.coastaleng.2007.12.003
- Camus, P., Menéndez, M., Méndez, F. J., Izaguirre, C., Espejo, A., Cánovas, V., et al. (2014). A weather-type statistical downscaling framework for ocean wave climate. Journal of Geophysical Research, Oceans, 119, 7389–7405. https://doi.org/10.1002/2014JC010141
- Codiga, D. (2011). Unified tidal analysis and prediction using the UTide Matlab functions.
- D'Anna, M., Idier, D., Castelle, B., Rohmer, J., Cagigal, L., & Mendez, F. J. (2022). Effects of stochastic wave forcing on probabilistic equilibrium shoreline response across the 21st century including sea-level rise. Coastal Engineering, 175, 104149. https://doi.org/https://doi.org/10.1016/j.coastaleng.2022.104149
- Dundas, S. J., & Lewis, D. J. (2020). Estimating Option Values and Spillover Damages for Coastal Protection: Evidence from Oregon's Planning Goal 18. Journal of the Association of Environmental and Resource Economists, 7(3), 519-554. https://doi.org/10.1086/708092
- Durrant, T., Greenslade, D.J.M., Hemer, M. and Trenham, C. (2014) A global wave hindcast focussed on the Central and South Pacific. CAWCR Technical Report No. 070. Melbourne. Retrieved from http://www.cawcr.gov.au/technical-reports/CTR_070.pdf
- Erikson, L., Morim, J., Hemer, M., Young, I., Wang, X. L., Mentaschi, L., . . . Webb, A. (2022). Global ocean wave fields show consistent regional trends between 1980 and 2014 in a multi-product ensemble. Communications Earth & Environment, 3(1), 320.

- https://doi.org/10.1038/s43247-022-00654-9 Hadziomerspahic, A. (2022). Valuing Coastal Risk with Revealed and Stated Preference Methods, (Doctoral dissertation). Corvallis, Oregon: Oregon State University.
- Hamdi, Y., Haigh, I. D., Parey, S., & Wahl, T. (2021). Preface: Advances in extreme value analysis and application to natural hazards. Nat. Hazards Earth Syst. Sci., 21(5), 1461-1465. https://doi.org/10.5194/nhess-21-1461-2021
- Hibbard, K. A., & Janetos, A. C. (2013). The regional nature of global challenges: a need and strategy for integrated regional modeling. Climatic Change, 118(3-4), 565-577. https://doi.org/10.1007/s10584-012-0674-3
- Hinkel, J., Feyen, L., Hemer, M., Le Cozannet, G., Lincke, D., Marcos, M., . . . Wolff, C. (2021). Uncertainty and Bias in Global to Regional Scale Assessments of Current and Future Coastal Flood Risk. Earths Future, 9(7), e2020EF001882. https://doi.org/10.1029/2020EF001882
- Holman, R. A. (1986). "Extreme value statistics for wave run-up on a natural beach." Coastal Engineering 9(6): 527-544. doi:https://doi.org/10.1016/0378-3839(86)90002-5
- Huang, B., Banzon, V. F., Freeman, E., Lawrimore, J., Liu, W., Peterson, T. C., . . . Zhang, H.-M. (2015). Extended Reconstructed Sea Surface Temperature Version 4 (ERSST.v4). Part I: Upgrades and Intercomparisons. Journal of Climate, 28(3), 911-930. https://doi.org/https://doi.org/10.1175/JCLI-D-14-00006.1
- Kates, R.W., Clark, W.C., Corell, R., Hall, J.M., Jaeger, C.C., Lowe, I., McCarthy, J.J., Schellnhuber, H.J., Bolin, B., Dickson, N.M. & Faucheux, S. (2000). Sustainability Science Research and Assessment Systems for Sustainability Program Discussion Paper 2000-33. Environment and Natural Resources Program, Belfer Centre for Science and International Affairs, Harvard University.
- Komar, P., Allan, J. & Ruggiero, P. (2011) Sea level variations along the US Pacific Northwest coast: Tectonic and climate controls. J. of Coast. Res. 27(5), 808–823.
- Komar, P.D., Allan, J.C., Ruggiero, P. (2013). U.S. Pacific Northwest Coastal Hazards: Tectonic and Climate Controls. In: Finkl, C. (eds) Coastal Hazards. Coastal Research Library, vol 1000. Springer, Dordrecht. https://doi.org/10.1007/978-94-007-5234-4 21
- Kopp, R. E., Gilmore, E. A., Little, C. M., Lorenzo-Trueba, J., Ramenzoni, V. C., & Sweet, W. V. (2019). Usable Science for Managing the Risks of Sea-Level Rise. Earth's Future. https://doi.org/10.1029/2018ef001145
- Laird, A. (2018). Humboldt Bay Area Plan: Sea Level Rise Vulnerability Assessment, Humboldt County. Retrieved from: https://humboldtgov.org/DocumentCenter/View/62872/Humboldt-Bay-Area-Plan-Sea-Level-Rise-Vulnerability-Assessment-Report-PDF?bidId=
- Le Cozannet, G., Castelle, B., Ranasinghe, R., Wöppelmann, G., Rohmer, J., Bernon, N., et al. (2019). Quantifying uncertainties of sandy shoreline change projections as sea level rises. Sci. Rep. 9:42. doi: 10.1038/s41598-018-37017-4
- Light, J. (2021). Morphodynamic evolution of coastal Oregon: using new lidar-derived beach and sand dune morphometrics to explore multi-decadal change, (M.S. thesis). Corvallis, Oregon: Oregon State University.

- Lipiec, E., Ruggiero, P., Mills, A., Serafin, K. A., Bolte, J., Corcoran, P., . . . Lach, D. (2018). Mapping Out Climate Change: Assessing How Coastal Communities Adapt Using Alternative Future Scenarios. Journal of Coastal Research, 34(5). https://doi.org/10.2112/jcoastres-d-17-00115.1
- Marra, J. J., Sweet, W. V., Leuliette, E., Kruk, M., Genz, A. S., Storlazzi, C. D., . . . Chiesa, C. Advancing Best Practices for the Analysis of the Vulnerability of Military Installations in the Pacific Basin to Coastal Flooding under a Changing Climate RC-2644: Final Report for the U.S. Department of Defense Strategic Environmental Research and Development Program. June 1, 2022. 543pp.
- Martello, M. V., & Whittle, A. J. (2023). Estimating coastal flood damage costs to transit infrastructure under future sea level rise. Communications Earth & Environment, 4(1), 137. https://doi.org/10.1038/s43247-023-00804-7
- Mills, A. K., Ruggiero, P., Bolte, J. P., Serafin, K. A., & Lipiec, E. (2021). Quantifying Uncertainty in Exposure to Coastal Hazards Associated with Both Climate Change and Adaptation Strategies: A U.S. Pacific Northwest Alternative Coastal Futures Analysis. Water, 13(4). https://doi.org/10.3390/w13040545
- Mills, M., Leon, J. X., Saunders, M. I., Bell, J., Liu, Y., O'Mara, J., . . . Hoegh-Guldberg, O. (2015). Reconciling Development and Conservation under Coastal Squeeze from Rising Sea Level. Conservation Letters, 9(5), 361-368. https://doi.org/10.1111/conl.12213
- Moftakhari, H. R., AghaKouchak, A., Sanders, B. F., Feldman, D. L., Sweet, W., Matthew, R. A., & Luke, A. (2015). Increased nuisance flooding along the coasts of the United States due to sea level rise: Past and future. Geophysical Research Letters, 42(22), 9846-9852. https://doi.org/10.1002/2015gl066072
- Morim, J., Wahl, T., Vitousek, S., Santamaria-Aguilar, S., Young, I., & Hemer, M. (2023). Understanding uncertainties in contemporary and future extreme wave events for broad-scale impact and adaptation planning. Science Advances, 9. https://doi.org/10.1126/sciadv.ade3170
- Norström, A. V., Cvitanovic, C., Löf, M. F., West, S., Wyborn, C., Balvanera, P., . . . Österblom, H. (2020). Principles for knowledge co-production in sustainability research. Nature Sustainability, 3(3), 182-190. https://doi.org/10.1038/s41893-019-0448-2
- Oppenheimer, M., Glavovic, B. C., Hinkel, J., Wal, R. v. d., Magnan, A. K., Abd-Elgawad, A., . . . Sebesvari, Z. (2019). Sea Level Rise and Implications for Low-Lying Islands, Coasts and Communities (IPCC Special Report on the Ocean and Cryosphere in a Changing Climate, Issue.
- Otto, I. M., Reckien, D., Reyer, C. P. O., Marcus, R., Le Masson, V., Jones, L., . . . Serdeczny, O. (2017). Social vulnerability to climate change: a review of concepts and evidence. Regional Environmental Change, 17(6), 1651-1662. https://doi.org/10.1007/s10113-017-1105-9
- Oregon Seismic Safety Policy Advisory Commission (OSSPAC) (2013). The Oregon Resilience Plan, Reducing Risk and Improving Recovery for the Next Cascadia Earthquake and Tsunami. Report to the 77th Legislative Assembly, Salem, Oregon. 306pp. https://digitalcommons.humboldt.edu/hsuslri_local/5

- Perez, J., Méndez, F. J., Menéndez, M., & Losada, I. J. (2014). ESTELA: A method for evaluating the source and travel time of the wave energy reaching a local area. Ocean Dynamics, 64(8), 1181–1191. https://doi.org/10.1007/s10236-014-0740-7
- Pullen, T., Allsop, W., Bruce, T., Kortenhaus, A., Schüttrumpf, H., & van der Meer, J. (2007). EurOtop Wave Overtopping of Sea Defences and Related Structures: Assessment Manual.
- Quinalt Indian Nation (2017). The Taholah Village Relocation Master Plan. C. D. a. P. Department, Quinalt Indian Nation Business Committee. Retrieved from: https://www.quinaultindiannation.com/planning/FINAL_Taholah_Relocation_Plan.pdf
- Roelvink, D., Reniers, A., van Dongeren, A., van Thiel de Vries, J., McCall, R., & Lescinski, J. (2009). Modelling storm impacts on beaches, dunes and barrier islands. Coastal Engineering, 56(11), 1133-1152. https://doi.org/https://doi.org/10.1016/j.coastaleng.2009.08.006
- Ruckelshaus Center (2017). Washington State Coast Resilience Assessment: Final Report, May 1, 2017. Retrieved from: http://ruckelshauscenter.wsu.edu/wp-content/uploads/sites/74/2013/06/Washington-Coast-Resilience-Assessment-Report_Final_5.1.17.pdf
- Ruggiero, P., Hacker, S., Seabloom, E., Zarnetske, P. (2018). The Role of Vegetation in Determining Dune Morphology, Exposure to Sea-Level Rise, and Storm-Induced Coastal Hazards: A U.S. Pacific Northwest Perspective. In: Moore, L., Murray, A. (eds) Barrier Dynamics and Response to Changing Climate. Springer, Cham. https://doi.org/10.1007/978-3-319-68086-6_11
- Ruggerio, P., Kratzmann, M. G., Himmelstoss, E. A., Reid, D., Allan, J., & Kaminsky, G. (2013). National assessment of shoreline change: historical shoreline change along the Pacific Northwest coast [Report](2012-1007). (Open-File Report, Issue. U. S. G. Survey. https://pubs.usgs.gov/publication/ofr20121007
- Saha, S., Moorthi, S., Wu, X., Wang, J., Nadiga, S., Tripp, P., et al. (2011). NCEP Climate Forecast System Version 2 (CFSv2) Selected Hourly Time-Series Products. Research data archive at the National Center for Atmospheric Research, Computational and Information Systems Laboratory. https://doi.org/10.5065/D6N877VB
- Sallenger, A. H. (2000). "Storm Impact Scale for Barrier Islands." Journal of Coastal Research 16(3): 890-895
- Serafin, K. A., & Ruggiero, P. (2014). Simulating extreme total water levels using a time-dependent, extreme value approach. Journal of Geophysical Research: Oceans, 119(9), 6305-6329. https://doi.org/10.1002/2014jc010093
- Serafin, K. A., Ruggiero, P., & Stockdon, H. F. (2017). The relative contribution of waves, tides, and nontidal residuals to extreme total water levels on U.S. West Coast sandy beaches. Geophysical Research Letters, 44(4), 1839-1847. https://doi.org/10.1002/2016gl071020
- Serafin, K. A., Ruggiero, P., Barnard, P. L., & Stockdon, H. F. (2019). The influence of shelf bathymetry and beach topography on extreme total water levels: Linking large-scale changes of the wave climate to local coastal hazards. Coastal Engineering, 150, 1-17. https://doi.org/https://doi.org/10.1016/j.coastaleng.2019.03.012

- Shope, J.B., Erikson, L.H., Barnard, P.L., Storlazzi, C.D., Hardy, M.W., and Doran, K.S. (2021). Modeled extreme total water levels along the U.S. west coast: U.S. Geological Survey data release, https://doi.org/10.5066/P95FBGZ1.
- Shope, J. B., Erikson, L. H., Barnard, P. L., Storlazzi, C. D., Serafin, K., Doran, K., . . . Ruggiero, P. (2022). Characterizing storm-induced coastal change hazards along the United States West Coast. Scientific Data, 9(1), 224. https://doi.org/10.1038/s41597-022-01313-6
- Smith, G. A., Hemer, M., Greenslade, D., Trenham, C., Zieger, S., & Durrant, T. (2020). Global wave hindcast with Australian and Pacific Island Focus: From past to present. Geoscience Data Journal, 8, 1–33. https://doi.org/10.1002/gdj3.104
- Splinter, K. D., & Coco, G. (2021). Challenges and Opportunities in Coastal Shoreline Prediction. Frontiers in Marine Science, 8. https://doi.org/10.3389/fmars.2021.788657
- Staisch, L.M., & Walton, M.A. (2022). Cascadia subduction zone database: compilation of published datasets relevant to Cascadia subduction zone earthquake hazards and tectonics: U.S. Geological Survey data release, https://doi.org/10.5066/P9069X6E.
- Stanton, K. A., & Tilt, J. H. (2023). Building resilient Oregon coastal communities: Reimagining critical facilities through Latinx sense of place. International Journal of Disaster Risk Reduction, 87, 103600. https://doi.org/https://doi.org/10.1016/j.ijdrr.2023.103600
- Stockdon, H. F., Holman, R. A., Howd, P. A., & Sallenger, A. H. (2006). Empirical parameterization of setup, swash, and runup. Coastal Engineering, 53(7), 573-588. https://doi.org/https://doi.org/10.1016/j.coastaleng.2005.12.005
- Sweet, W. V., Hamlington, B. D., Kopp, R. E., Weaver, C. P., Barnard, P. L., Bekaert, D., ... & Zuzak, C. (2022). Global and regional sea level rise scenarios for the United States: Updated mean projections and extreme water level probabilities along US coastlines. National Oceanic and Atmospheric Administration.
- Taherkhani, M., Vitousek, S., Barnard, P. L., Frazer, N., Anderson, T. R., & Fletcher, C. H. (2020). Sea-level rise exponentially increases coastal flood frequency. Scientific Reports, 10(1), 6466. https://doi.org/10.1038/s41598-020-62188-4
- Thompson, V., Mitchell, D., Hegerl, G. C., Collins, M., Leach, N. J., & Slingo, J. M. (2023). The most at-risk regions in the world for high-impact heatwaves. Nat Commun, 14(1), 2152. https://doi.org/10.1038/s41467-023-37554-1
- Tillotson, K., & Komar, P. (1997). The Wave Climate of the Pacific Northwest (Oregon and Washington): A Comparison of Data Sources. Journal of Coastal Research, Vol. 13, 440-452.
- Toimil, A., Losada, I. J., Nicholls, R. J., Dalrymple, R. A., & Stive, M. J. F. (2020). Addressing the challenges of climate change risks and adaptation in coastal areas: A review. Coastal Engineering, 156. https://doi.org/10.1016/j.coastaleng.2019.103611
- Toimil, A., Camus, P., Losada, I. J., & Alvarez-Cuesta, M. (2021). Visualising the Uncertainty Cascade in Multi-Ensemble Probabilistic Coastal Erosion Projections [Original Research]. Frontiers in Marine Science, 8. https://doi.org/10.3389/fmars.2021.683535

- Toimil, A., Losada, I. J., Álvarez-Cuesta, M., & Le Cozannet, G. (2023). Demonstrating the value of beaches for adaptation to future coastal flood risk. Nature Communications, 14(1), 3474. https://doi.org/10.1038/s41467-023-39168-z
- van der Meer, J.W., 2002, Technical report wave run-up and wave overtopping at dikes: Deflt, Netherlands, Technical Advisory Committee on Flood Defence, Road and Hydraulic Engineering Institute, 50 p.
- Vitousek, S., Barnard, P. L., Fletcher, C. H., Frazer, N., Erikson, L., & Storlazzi, C. D. (2017). Doubling of coastal flooding frequency within decades due to sea-level rise. Scientific Reports, 7(1), 1399. https://doi.org/10.1038/s41598-017-01362-7
- Vitousek, S., Cagigal, L., Montaño, J., Rueda, A., Mendez, F., Coco, G., & Barnard, P. L. (2021). The Application of Ensemble Wave Forcing to Quantify Uncertainty of Shoreline Change Predictions. Journal of Geophysical Research: Earth Surface, 126(7). https://doi.org/10.1029/2019jf005506
- Vos, K., Harley, M. D., Turner, I. L., & Splinter, K. D. (2023). Pacific shoreline erosion and accretion patterns controlled by El Niño/Southern Oscillation. Nature Geoscience, 16(2), 140-146. https://doi.org/10.1038/s41561-022-01117-8
- Vousdoukas, M. I., Mentaschi, L., Voukouvalas, E., Verlaan, M., Jevrejeva, S., Jackson, L. P., & Feyen, L. (2018). Global probabilistic projections of extreme sea levels show intensification of coastal flood hazard. Nature Communications, 9(1), 2360. https://doi.org/10.1038/s41467-018-04692-w
- Vousdoukas, M. I., Ranasinghe, R., Mentaschi, L., Plomaritis, T. A., Athanasiou, P., Luijendijk, A., & Feyen, L. (2020). Sandy coastlines under threat of erosion. Nature Climate Change, 10(3), 260-263. https://doi.org/10.1038/s41558-020-0697-0
- Wahl, T., Haigh, I. D., Nicholls, R. J., Arns, A., Dangendorf, S., Hinkel, J., & Slangen, A. B. A. (2017). Understanding extreme sea levels for broad-scale coastal impact and adaptation analysis. Nature Communications, 8(1), 16075. https://doi.org/10.1038/ncomms16075
- Wheeler, M. C., & Hendon, H. H. (2004). An All-Season Real-Time Multivariate MJO Index: Development of an Index for Monitoring and Prediction. Monthly Weather Review, 132(8), 1917-1932. https://doi.org/https://doi.org/10.1175/1520-0493(2004)132<1917:AARMMI>2.0.CO;2
- Wood, N. J., Burton, C. G., & Cutter, S. L. (2010). Community variations in social vulnerability to Cascadia-related tsunamis in the U.S. Pacific Northwest. Natural Hazards, 52(2), 369-389. https://doi.org/10.1007/s11069-009-9376-1



Earth's Future

Supporting Information for

Projecting Future Chronic Coastal Hazard Impacts, Hotspots, and Uncertainty at Regional Scale

Meredith Leung¹, Laura Cagigal², Fernando Mendez², Peter Ruggiero¹

¹College of Earth, Ocean, and Atmospheric Sciences, Oregon State University, Corvallis, OR, USA ²Departamento Ciencias y Tecnicas del Agua y del Medio Ambiente, Universidad de Cantabria, Santander, Spain

Corresponding author: Meredith Leung (leungmer@oregonstate.edu)

Contents of this file

Text S1 to S2 Figures S1 to S2

S1. Methodology for Semi-Coupling TESLA Nodes.

In the TESLA lexicon, the term 'semi-coupled' indicates that multiple TESLA nodes share model predictors (i.e., weather types: AWTs, IWTs, and DWTs), while each node maintains unique predictands (wave characteristics and water level drivers). To semi-couple AWTs and IWTs is trivial for the Cascadia nodes, as AWTs (representing ENSO patterns) are universal for the entire Pacific Basin and IWTs (representing MJO cycles) are universal for the entire globe. DWTs, representing synoptic weather, are tailored for each site, so the semi-coupling methodology requires a few additional steps and is detailed below.

The methodology to create DWTs for a single site in TESLA involves using the model ESTELA (Evaluation of Source and Travel-time of wave Energy reaching a Local Area; Perez et al., 2014) to define a bounding region representing the area from which 99% of wave energy traveling along great circle arcs reaches the study site. SLP, representing high and low-pressure systems in the atmosphere, and SLP gradients, representing the wind stress responsible for generating waves and storm surge, from CFSR reanalysis products (Saha et al., 2011) are extracted from within the ESTELA bounds. Weather typing, which consists of principal component analysis of SLP and SLPG datasets and k-means clustering of resultant principal components, is performed at daily scale to depict patterns of synoptic weather in the region of interest. More detail on this methodology can be found in Anderson et al. (2019) and Camus et al. (2014).

If this methodology were completed at each of the eight Cascadia nodes independently, DWTs would likely be similar but not exactly the same, as slightly different ESTELA boundaries would be defined and the k-means clustering algorithm inserts some inherent randomness in the weather typing process. To ensure synoptic weather is represented uniformly across all eight nodes, we defined ESTELA bounds for three of our eight TESLA nodes (the northern-most, southern-most, and central-most study sites) and created a combined boundary that envelopes the largest extent of all three bounds (Figure S1). SLP and SLP gradient extraction and subsequent weather typing was performed using the central-most site as the anchoring point following the Anderson et al. (2019) methodology and used as the DWTs for all eight nodes.

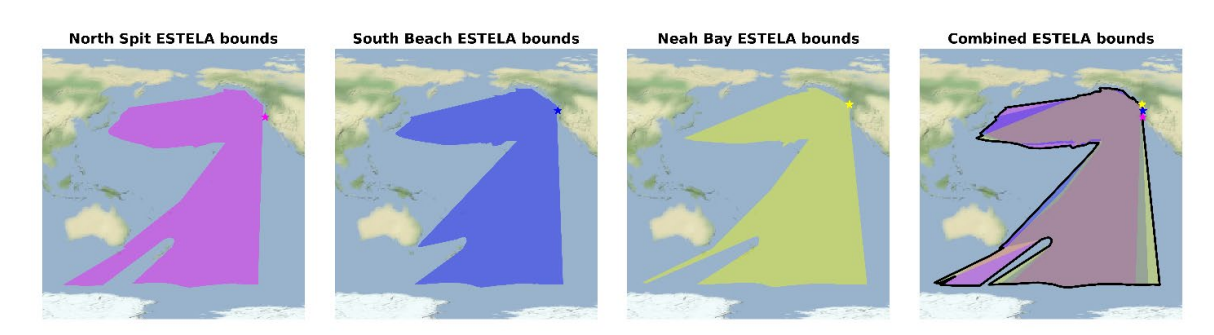


Figure S1. Area where 99% of wave energy reaching the specified site is generated according to ESTELA. Wave energy boundaries for three (northernmost, central, and southernmost) TESLA nodes were combined to form a super-boundary. Sea level pressure and sea level pressure gradients are extracted from the boundaries and used to define the

DWTs for the Cascadia region, enabling coupling of WTs for all TESLA sites, while maintaining independent hydrodynamic variables.

S2. Simplification of Hazard Probability Space for Regional Scale Analysis

Due to the high resolution and dimensionality of the hazard proxy data (~9,000 transects, 800,000+ hours, 3 SLR scenarios, 100 simulations), it was necessary to reduce the computational expense of our analysis before assessing hazard impacts on the regional scale. To do this, we calculated the likelihood that a hazard impact occurred for each hour over the 100 simulations using binomial maximum likelihood estimates (MLEs) for the 0.05, 0.5, and 0.95 cases. Calculating the binomial MLEs for median and tail cases allows us to represent the probability distribution of hazard impact without saving the entire distribution, while still exploring hazard impacts at the full spatial and temporal resolution of the dataset. The hazard proxy data is instead represented by ~9,000 transects, 800,000+ hours, 3 SLR scenarios, and 3 MLEs. The binomial MLEs representing the tails (0.05, 0.95) and median (0.50) cases of TWL variability are then used to calculate the percent occurrence (eq. 3) and hotspot change indices (eqs. 4, 5) at each transect and at the different time intervals of interest.

Using the three MLEs to represent the hazard impact probability space rather than the 100 simulations minimally alters how the tails of the percent occurrence results are represented based on which time interval being explored. The effect of using the MLEs rather than the full simulation space can be seen in figure S1, where we show the beach safety percent occurrence for the same transect shown in figure 6. The percent occurrence from the median (0.50) MLE matches the median percent occurrence found from using the full simulation space at all time durations explored (the interpretation of median probability hazard occurrence is not affected). However, the 0.05 and 0.95 binomial MLEs represent different quantiles than the full simulation space when calculating the percent occurrence for different time durations. At the monthly time scale, the 0.05 and 0.95 MLEs percent occurrence aligns well with the inter-quartiles of the full simulation space. At the annual time scale, the 0.05 and 0.95 MLEs match well with the 0.05 and 0.95 guantiles, and at the decadal scale the 0.05 and 0.95 MLEs represent outliers of the full simulation and time space since they retain more information from the hourly scale. In short, the tails of the hazard occurrence probability space are represented differently by the 0.05 and 0.95 MLEs when assessing different time periods.

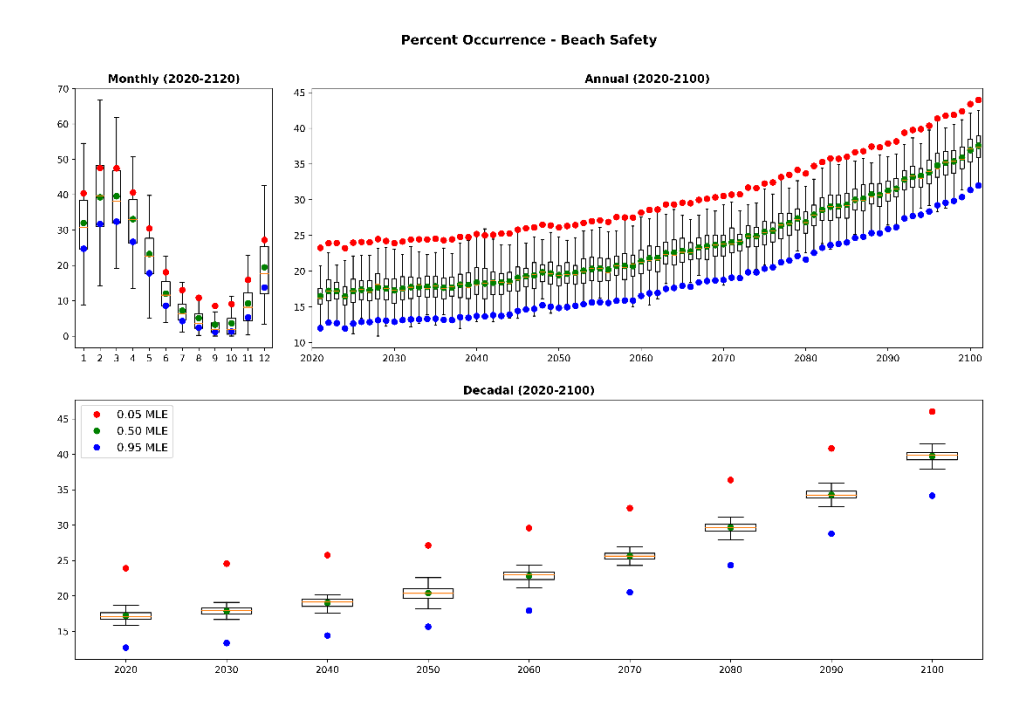


Figure S2. Box plots of unsafe beach percent occurrence compared to the percent occurrence of the 0.05, 0.5, 0.95 binomial MLEs derived from the 100 TWL simulations for one transect (same transect shown in figure 6).